

# Scaling of Particle Trajectories on a Lattice I: Critical Behavior

Mei-She Cao and E.G.D. Cohen

The Rockefeller University

1230 York Avenue, New York, NY 10021

May 7, 2019

## Abstract

The scaling behavior of the closed trajectories of a moving particle generated by randomly placed rotators or mirrors on a square or triangular lattice is studied numerically. For most concentrations of the scatterers the trajectories close exponentially fast. For special critical concentrations infinitely extended trajectories can occur which exhibit a scaling behavior similar to that of the perimeters of percolation clusters. In addition to the two critical exponents  $\beta = 15/7$  and  $d_f = 7/4$  found before, the critical exponent  $\gamma = 3/7$ , which is associated with the scaling function for trajectory size away from criticality, also appears. This exponent determines structural scaling properties of closed trajectories of finite size when they approach infinity, at criticality. New scaling behavior was found for the square lattice partially occupied by rotators, indicating a different universality class from that of percolation clusters. An argument for the scaling behavior found along the critical lines is presented.

**Key words:** Lattice, particle trajectories, percolation, scaling, criticality.

# 1 Introduction

In a number of previous publications<sup>(1-10)</sup>, the diffusion properties of Lorentz lattice gas cellular automata (LLGCA) has been studied. There the behavior of a point particle moving through fixed, regularly<sup>(6)</sup> or randomly<sup>(1, 5, 7-10)</sup> placed scatterers on the lattice sites of a variety of planar lattices has been studied numerically. The scatterers consisted either of reflecting right and left mirrors or of rotating right and left rotators, which scatter the particle either to its right or its left, respectively (Fig. 1-2). The particle is constrained to move in unit time steps along the lattice bonds (of unit length) and the lattices studied were the square<sup>(1,2,4,7)</sup>, triangular<sup>(3,7)</sup>, honeycomb<sup>(8)</sup>, quasi-lattice<sup>(8)</sup> and random lattice<sup>(3,9)</sup>. Since these scatterers are fixed on the lattice, the particle simply travels periodically in the plane once the trajectory forms a closed orbit. In our computer simulations, the particle is stopped right after the first period. In almost all cases studied so far, all the trajectories close exponentially fast. However, in some cases they close power law slow. While in the former case all orbits appear to close after typically  $2^{10}$  time steps, in the latter case there are extended trajectories, possibly of infinite length, which only close after a long (possibly infinite) time. Studying these extended trajectories reveals that they exhibit scaling properties, which in the case of a lattice fully occupied by scatterers, can be mapped onto a corresponding bond or site percolation problem. However, in the case of a lattice not fully occupied by scatterers, where empty sites occur and the particle trajectory can cross itself, no such mapping seems possible. Nevertheless some of the scaling properties of these trajectories are then still the same as those found for the fully occupied lattice where no such crossing can occur (Fig. 3). The identity of the scaling properties of the closed trajectories with those of a corresponding percolation problem is exemplified, for example, by the appearance of the same two universal critical exponents that occur in the two dimensional (bond or

site) percolation problem : a fractal dimension  $d_f = 7=4$  associated with the length  $S$  of the trajectories (perimeter of the percolation cluster) and the mean square distance of all points on a large trajectory of length  $S$  from the origin,  $R_S^2$ ,

$$R_S^2 \propto S^{2=d_f} \quad (1)$$

as well as the Fisher exponent  $\alpha = 15=7$ , characterizing the probability distribution of closed trajectories of a certain length,

$$n_S \propto S^{-\alpha+1} \quad (2)$$

A hyperscaling relation holds between these exponents:

$$\alpha = \frac{2}{d_f} \quad (3)$$

We note that the closed particle trajectories, when mapped onto percolation clusters, are characterized here by their 'surface' properties, i.e., their length, not, as is usually done, by their 'bulk' properties, i.e., the total number of lattice sites they contain. The exact values for  $d_f$  were first conjectured to be  $4=7$  by Sapoval, Rosso, and Gouyet<sup>(11)</sup>. Ziff<sup>(12)</sup>, then, developed a scaling theory which implied that  $\alpha$  should be  $15=7$  and he verified numerically the values of  $d_f$  and  $\alpha$ . Later the conjecture was proved by Saleur and Duplantier<sup>(9)</sup> by mapping the percolation problem onto a Coulomb gas. However, for the partially occupied lattice at criticality, there is no theoretical explanation for the universality of  $\alpha$  and  $d_f$ .

In this and the following paper, we introduce finer characterizations of the closed particle trajectories than we have done in previous publications, where only the trajectory size distribution scaling exponent  $\alpha$  and the trajectory's fractal dimension  $d_f$  were considered. The quantities that describe the finer characterizations are: (1) The number of right, left scatterers and empty sites on a closed trajectory, i.e.  $N_R$ ,  $N_L$  and  $N_E$ , respectively; (2) The winding

angle  $W$ , i.e. the number of right turns minus the number of left turns of the particle moving on a closed trajectory; (3) The frequency with which lattice sites on the particle trajectory are visited by the moving particle. These are more detailed "structural" properties than the "gross" properties incorporated in  $\langle \dots \rangle_c$  and  $\langle \dots \rangle_{cc}$ . By studying these properties for finite trajectories of increasing length at criticality, we derive, in this paper, a number of trajectory scaling properties which include not only the asymptotic behavior for infinitely large closed trajectories, but also the approach to the asymptotic behavior. As an example of the new properties that we have just introduced, we quote one that occurs on the fully occupied square lattice, where each site is occupied either by a right or by a left rotator. If  $N_R$  and  $N_L$  are the numbers of right rotators and left rotators contained in a closed trajectory respectively, asymptotically  $N_R$  and  $N_L$  satisfy:

$$\left\langle \frac{N_R}{N} - \frac{1}{2} \right\rangle_c = \left\langle \frac{N_L}{N} - \frac{1}{2} \right\rangle_{cc} \sim N^{-0.57} \quad (4)$$

where  $N = N_R + N_L$  is the total number of sites of the closed trajectory. The averages  $\langle \dots \rangle_c$  and  $\langle \dots \rangle_{cc}$  are taken over all closed trajectories containing  $N$  sites in which the particle moves clockwise (Fig. 3) and counter-clockwise, respectively. There are two observations to make with regards to Eq. (4). First, the number of right and left rotators on a closed orbit become asymptotically equal, i.e. asymptotically  $N_R = N_L = 1/2$ . Second the critical exponent 0.57 is in good approximation equal to  $1/\nu = 3/7$ . All scaling results observed so far for the fully occupied square as well as triangular lattice are of the form of Eq.(4), where the constant inside the average (here equal to the critical concentration  $C_R = C_L = 1/2$ ) can vary, while for the partially occupied lattice the exponent 0.57 can change to its mean field value 0.50. In the context of Eq. (4), the difference of 0.57 and 0.50 means that asymptotically the right and left rotators are almost but not quite randomly distributed over the trajectory,

which is not surprising, since some correlations between the placing of right and left rotators on the lattice sites to generate a closed trajectory, would be expected. Surprising, though, is the universality of the exponent of 0.57, for which we have, at present, no explanation.

Another interesting feature is that some sites on the trajectories are only visited once by the moving particle and others can be visited more than once. The number of sites visited by the moving particle a different number of times exhibits a power law behavior similar to Eq. (4), except for the square lattice partially occupied by rotator scatterers, where the scaling behavior differs significantly from all other cases.

The numerical algorithm we used was obtained from an efficient combination of the Zi algorithm <sup>(4;12;14)</sup> (use of a virtual lattice) and a technique recently developed by Wang and Cohen <sup>(7;8)</sup> (dynamical memory allocation). The simulation was done on a virtual lattice of size 65536 × 65536. The lattice was divided into 1024 × 1024 blocks of 64 × 64 sites rather than 256 × 256 blocks of 256 × 256 sites as used by Zi <sup>(4)</sup> and Wang and Cohen <sup>(7;8)</sup>, since a smaller block size is more efficient for dilute scatterer models. 16 bits ( $2^{16} = 65536$ ) were used to determine the coordinates (x; y) of a site, the upper 10 bits ( $2^{10} = 1024$ ) were used for the location of the block which had been visited by the moving particle, while the lower 6 bits ( $2^6 = 64$ ) were used for the site position within the block. Another array of 1024 × 1024 was introduced, to record whether a block had been visited by the particle. The application of bit shifting, masking etc. to look up the coordinates of blocks and sites contained in the blocks made the whole process very fast. Furthermore, we used a dynamic memory allocation technique, where an array of pointers is generated so that each block has a corresponding pointer and actual memory of the states of the sites (i.e. the type of scatterers placed on the site) in the block is not assigned to its pointer until the particle enters it (using `malloc`

in C). After a trajectory is finished, only memories that have been assigned to the pointers are deleted (using FREE in C).

The advantage of this scheme is that since large trajectories are essentially fractals with fractal dimension  $d_f = 7/4$ , only a small fraction of the memory for a 65536 x 65536 array is actually used and we do not need to reserve memory for those areas that are never visited by the particle. Note that since the fluctuations in size of the trajectories are very big, our dynamic memory allocation technique saves an enormous amount of memory. For example, only a small array is generated for a small trajectory no matter how large other trajectories are. After the trajectory is completed, only the blocks that have been entered by the trajectories need to be reset to the blank condition so that another independent particle can be launched, rather than resetting the entire lattice. Therefore the average time required for this operation is significantly reduced. Since the memory is allocated dynamically, we do not need to know how much memory the largest trajectory requires before we start our numerical simulations.

About 300,000 independent particles, initially placed randomly on the lattice, were studied. We only collect closed particle trajectories whose lengths are smaller than a certain limit. The trajectory is disregarded if it did not close by that number of steps. The value of the limit we used was up to  $2^{21}$  -  $2^{24}$  time steps, depending on the concentration of the scatterers. In all the simulations, there was no particle that crossed the boundary of the virtual lattice.

We have verified for the fully occupied square lattice that our calculations have been made for systems of a sufficiently large number of particles and for sufficiently long times that the error bars in our figures are typically of the order of the size of the symbols. The same obtains for the fully occupied triangular lattice. However, for the partially occupied square and triangular

lattices the accuracy of our calculations decreases with the concentration of scatterers.

The organization of this paper is as follows. In section 2, we introduce the rotator model on the square lattice and discuss the closed trajectory scaling results for the rotator model both for a fully and for a partially occupied lattice. In section 3, the same is done for the mirror model. In section 4, we discuss the closed trajectory scaling results for the triangular lattice, which are the same for both the rotator and the mirror model, since they can be mapped in to each other for this lattice<sup>(3,7)</sup>. Section 5 contains a summary of our results in three tables as well as a discussion and an outlook. In the following paper scaling results, in particular the scaling function, describing the scaling behavior in the critical region near criticality will be given. The same exponent that played a dominant role in this paper at criticality, will also appear there.

## 2 Critical behavior of the rotator model on the square lattice

### 2.1 The fully occupied lattice

The rotator model is a special case of a general class of models, originally introduced by Gunn and Ortuño<sup>(15)</sup>. Fixed right (Fig. 1a) and left rotators (Fig. 1b) are randomly placed on the sites of the lattice. A particle moves along the bonds of the lattice and its velocity is rotated either to its right or to its left by  $\pi/2$  upon being scattered by a right or a left rotator, respectively (Fig. 3a). The total concentration of the scatterers  $C$  is the sum of those of the right rotators  $C_R$  and the left rotators  $C_L$ :  $C = C_R + C_L$ .

For the fully occupied lattice, i.e.  $C = 1$ , the trajectories of the moving particle can be mapped onto the perimeters of bond percolation clusters<sup>(4,7)</sup> which was first used by Grassberger<sup>(16)</sup>. A more detailed explanation about

this mapping will be presented in the following section by relating the rotator model to a mirror model. Since the critical concentration  $p_c$  for bond percolation on the square lattice is  $1=2$ , the critical concentration for the rotator model is also  $1=2$ , i.e.  $C_{R_c} = C_{L_c} = 1=2$ . Note that the right rotators are either on the outer side of the trajectories, in which case the trajectory is traversed clockwise, or on the inner side of the trajectories, in which case the trajectory is traversed counter-clockwise (Fig. 3a). It is convenient, in our numerical simulations, to introduce for the analysis of the trajectories the winding angle  $W$ , which, for example allows a determination of whether a closed trajectory is traversed clockwise or counter-clockwise. For a given trajectory,  $W$  is computed, at each step, by increasing it by  $=2$  if the particle is turned to the right, and decreasing it by  $=2$  if the particle is turned to the left. Then, when the trajectory closes, the winding angle will either be  $2$  or  $-2$  which corresponds to clockwise or counter-clockwise rotation, respectively, because trajectories cannot cross themselves.

Although we expect that, for large trajectories, the number of right rotators  $N_R$  and the number of left rotators  $N_L$  contained in the trajectories are on average the same, there are symmetric fluctuations of  $N_R = N$  with respect to the mean value  $C_{R_c} = 1=2$ . The distribution of  $N_R = N$  can be fitted to a double Gaussian (Fig. 4a). The symmetry is due to the fact that the same trajectory can be generated by replacing all right (left) rotators with left (right) rotators, respectively, and reversing the particle velocity. However, if we just look at the clockwise traversed trajectories, we find that the fluctuations of  $N_R = N$  are no longer symmetric with respect to  $1=2$  (Fig. 4b). This is not difficult to understand, because the right rotators are always on the outer side of the trajectories while the left rotators are always on the inner side of the trajectories. In other words, the symmetry between right rotators and left rotators is broken by our selection. From our numerical results, we found

that for most clockwise closed trajectories  $N_R > N_L$ , while in a few cases,  $N_R < N_L$  (Fig. 4b). As we increase the size of the trajectories, the average of the distribution of  $N_R$  and  $N_L$  shifts toward 1=2 with a power law (Fig. 5),

$$\langle \frac{N_R}{N} \rangle = 1=2 = \langle \frac{N_L}{N} \rangle = 1=2 \approx N^{-0.57} \quad (5)$$

It has been noticed before<sup>(4,9)</sup> that memory effects play a dominant role in the motion of the particle on the lattice with fixed scatterers and in the generation of its trajectory. However, no direct measurement of a memory effect has been given. In this paper, we do so for the rotator model, by examining how many sites on a trajectory are visited once  $N_1$  (no memory effect) and how many sites on the same trajectory are visited twice  $N_2$  (memory effect). A site on the trajectory can not be visited more than twice on the fully occupied lattice, since for a particle to return to the same site, it has to move an even number of steps. As at each step, the winding angle changes by  $\pi/2$ , the change of the winding angle can only be either  $\pi/2$  or  $-\pi/2$  when the particle returns to the same site, (Fig. 3), so that only  $N_1$  and  $N_2$  are allowed. Thus we have the following sum rule,

$$N_1 + N_2 = N \quad (6)$$

If  $S$  is the length of the trajectory, we also have,

$$N_1 + 2N_2 = S \quad (7)$$

Our numerical results show that (Fig. 6),

$$\langle \frac{N_1}{N} \rangle = \frac{1}{2} = \langle \frac{1}{2} \frac{N_2}{N} \rangle = N^{-0.57} \quad (8)$$

Note that  $N_1/N$  approaches 1=2 from above while  $N_2/N$  approaches 1=2 from below. i.e. for infinitely large trajectories  $N_1/N$  and  $N_2/N$  are equal. This implies that memory effects are indeed very important even for those trajectories whose length are infinitely large. The asymptotic value 1=2 for  $N_1/N$  and  $N_2/N$  was noticed independently by Zi<sup>(17)</sup>.

Besides the memory effect exhibited by  $N_1$  and  $N_2$ , there are other interesting structural properties associated with  $N_1$  and  $N_2$ . For each site belonging to  $N_1$ , only two out of four adjacent bonds belong to the trajectory, while for each site belonging to  $N_2$ , all four adjacent bonds belong to the trajectory (Fig. 3a), i.e. the site is surrounded by the trajectory (Fig. 3a). In other words, the  $N_1$  form the "surface" of a trajectory, while the  $N_2$  form the "bulk" of the trajectory. We want to point out that the "surface" and the "bulk" introduced here are different from the outer and inner sides we introduced earlier, since some sites on the outer side of a trajectory belong to  $N_2$  and some sites on the inner side of that trajectory belong to  $N_1$ .

Although Eq. (5) and Eq. (8) exhibit the same power law behavior, we have not obtained an explanation for this. From Eq. (6), Eq. (7) and Eq. (8), the following relation can be derived,

$$\left\langle \frac{S}{N} \right\rangle \frac{3}{2} \propto N^{-0.57} \quad (9)$$

indicating that  $S$  and  $N$  are asymptotically proportional to each other. Therefore, replacing  $S^{-0.57}$  by  $N^{-0.57}$  in all scaling equations is justified, as long as the asymptotic behavior is considered.

## 2.2 The partially occupied lattice

For a partially occupied lattice, the trajectories can cross themselves (Fig. 2a). The outer side and inner side of the closed orbits cannot be well defined anymore, so that a direct mapping of the trajectories onto the perimeters of bond percolation clusters is not possible<sup>(7,18)</sup>. Nevertheless earlier numerical studies<sup>(7)</sup> have still shown the existence of two critical lines symmetric with respect to the line  $C_R = C_L$  (Fig. 7) and the critical exponents,  $\alpha$  and  $d_f$  have the same values as at  $C = 1$ . However, the existence of these critical lines below  $C = 0.56$  could not be established, due to the prohibitively long

numerical calculations needed. We will give more details about some special features of the critical lines in the following paper.

One important consequence of the inequality of  $C_R$  and  $C_L$  at criticality for  $C < 1$  is that the winding angles are asymptotically proportional to the number of sites or to the number of time steps contained in the closed trajectories. As an example, we consider to the critical point at concentration  $C = 0.90$ , namely,  $C_R = 0.477$ ,  $C_L = 0.423$ . To our surprise, our numerical results exhibit that the deviation of the winding angle from its mean value ( $C_R - C_L$ ) decays not with a power law but with a stretched exponential law (Fig. 8),

$$\left\langle \frac{W(N)}{N} - (C_R - C_L) \right\rangle \sim 2^{(-2.8N^{0.18})} \quad (10)$$

For  $N_R = N$ ,  $N_L = N$  and  $N_E = N$ , our numerical calculations yield the following scaling relation (Fig. 9),

$$\left\langle \frac{N_R}{N} - C_R \right\rangle \sim \left\langle \frac{N_L}{N} - C_L \right\rangle \sim \left\langle \frac{N_E}{N} - C_E \right\rangle \sim N^{-0.50} \quad (11)$$

Note that the value of the exponent  $-0.50$  differs from that for the fully occupied lattice  $-0.57$ , indicating that self-crossing occurs randomly as the particle generates its trajectory.

The memory effects on the partially occupied lattice are more complicated than on the fully occupied lattice. For example, the number of times that a site can be visited by the moving particle can range from one to four. We denote the number of these different types of sites by  $N_1$ ,  $N_2$ ,  $N_3$  and  $N_4$ , respectively. An interesting feature for  $C < 1$  is that "re-actors" can be formed after a number of time steps on a trajectory (a "re-actor" is formed when the moving particle travels through the same bond as it has traveled on before, but in the opposite direction, Fig. 10). We remark here that these "re-actors", are responsible for the absence of diffusion for theipping rotator model as proved by Bunimovich and Troubetzkoy<sup>(19)</sup> and make  $N_3$  and  $N_4$  non

vanishing. Since each site belongs to only one of the four types,  $N_1, N_2, N_3$  or  $N_4$ , we have the following two sum rules,

$$N_1 + N_2 + N_3 + N_4 = N \quad (12)$$

and

$$N_1 + 2N_2 + 3N_3 + 4N_4 = S \quad (13)$$

These two relations are quite useful for numerical simulations, since for known  $N_1, N_2, N_3$  and  $S$ , one can find  $N_3$  and  $N_4$ , saving therefore a large amount of memory and computational time. If the asymptotic values for  $N_1=N$ ,  $N_2=N$ ,  $N_3=N$  and  $N_4=N$  are represented by  $K_1, K_2, K_3$  and  $K_4$ , respectively, our numerical simulations show the following power law behavior (Fig. 11),

$$\left\langle \frac{N_1}{N} \right\rangle K_1 > \left\langle \frac{N_2}{N} \right\rangle K_2 > \left\langle K_3 \right\rangle \frac{N_3}{N} > \left\langle K_4 \right\rangle \frac{N_4}{N} > N^{-0.39} \quad (14)$$

The sum of  $K_1, K_2, K_3$  and  $K_4$  is equal to one as required by Eq. (12). We found that  $K_1, K_2, K_3$  and  $K_4$  are functions of the concentration  $C$  and all converge to values near 1/4, (Fig. 12). The exponent -0.39 in the above equation is significantly different from the corresponding one for the fully occupied lattice -0.57, although  $d_f$  and  $d_f$  are still the same as found by Cohen and Wang<sup>(7)</sup>. The same scaling behavior is found at  $C = 0.80$ , suggesting that the critical behavior is universal along the critical line.

In the same way as was done for the fully occupied lattice, we can derive the scaling behavior for  $S=N$  from Eq. (12), (13) and (14),

$$\left\langle \frac{S}{N} \right\rangle 2.3670 > N^{-0.39} \quad (15)$$

We note that the sites that belong to  $N_2$  can be separated into two classes: those that only have three adjacent bonds traversed by the particle and those that have four adjacent bonds traversed by the particle. The former together with  $N_1$  form the 'surface' of the trajectories while the latter together with  $N_3$  and  $N_4$  form the 'bulk' of the trajectories.

### 3 Critical behavior of the mirror model on the square lattice

#### 3.1 The fully occupied lattice

The mirror model was proposed by Ruijgrok and Cohen sometime ago <sup>(1)</sup>, where the scatterers consist of right mirrors (tilted to the right by  $\pi/4$ , Fig. 1c) and left mirrors (tilted to the left by  $\pi/4$ , Fig. 1d), which reflect the particle upon collision, like a photon is reflected from a mirror.  $C_R$  and  $C_L$  are now the concentrations of right mirrors and left mirrors, respectively, and  $C = C_L + C_R$ . It has been shown before<sup>(4,7,20)</sup> that  $C = 1$  is a critical line for the mirror model. Only for  $C_R = C_L = 1/2$ , can the mirror model and the rotator model be mapped onto each other. That is, by properly replacing right mirrors and left mirrors with either left rotators or right rotators, we can produce the same trajectory with the same probability. For  $C_R \neq C_L$ , the trajectories can still be mapped onto each other, but the probability to generate the same trajectory by mirrors is no more the same as by rotators, so that these two models cannot be mapped onto each other anymore. However, we will show later in this section, that the mirror model can still be related to a rotator model, even when  $C_R \neq C_L$ .

The mirror model can, for all  $C = 1$ , still be mapped onto an isotropic bond percolation problem at criticality, (except in the two limits:  $C_R = 1, C_L = 0$ , and  $C_R = 0, C_L = 1$ , where the moving particle simply zig-zags to infinity). Therefore the trajectory length distribution, characterized by  $\langle \ell \rangle = 15.7$  and the fractal dimension  $d_f = 7/4$  are still the same as before. However,  $\langle \ell \rangle$  cannot be defined anymore for the mirror model at  $C = 1$ , because we are on a critical line rather than at a critical point, as was the case for the rotator model.

Unlike in the rotator model, in the mirror model right mirrors can either be on the outer or on the inner sides of a trajectory, therefore the method

of separating trajectories into clockwise and counter-clockwise ones will not break the symmetry between the number of right mirrors  $M_R$  and the number of left mirrors  $M_L$  on the trajectories. Indeed, our numerical results show that the distribution of  $M_R = N$  ( $N = M_R + M_L$ ) is a Gaussian centered at  $C_R$  rather than a double Gaussian as we found in the rotator model, Fig. 13. The following power law describes how this distribution narrows as  $N$  increases (Figs 13,14),

$$\langle \frac{M_R}{N} - C_R \rangle = \langle \frac{M_L}{N} - C_L \rangle \propto N^{-0.50} \quad (16)$$

The exponent 0.50 is not surprising here. The key point is that  $C = 1$  is a critical line, so that for a large trajectory, we cannot tell at which concentration it is generated. In other words, the number  $M_R = N$  can fluctuate freely about its mean value  $C_R$ . According to the central limit theorem, we get then the observed result.

Memory effects can be studied in the same way as for the rotator model, because each site on the trajectories can be only visited either once or twice, the same as for the fully occupied rotator model. Our numerical results show that the scaling behavior of  $N_1 = N$  and  $N_2 = N$  is the same as that for the rotator model, except that the asymptotic value now depends on the concentration  $C_R$ , (Fig. 15),

$$\langle \frac{N_1}{N} - a(C_R) \rangle = \langle b(C_R) - \frac{N_2}{N} \rangle \propto N^{-0.57} \quad (17)$$

From  $N_1 + N_2 = N$ , we have  $a(C_R) + b(C_R) = 1$ . For  $C_R > 1/2$ , our simulations show that,  $a(C_R)$  is monotonically decreasing with  $C_R$ , while for  $C_R < 1/2$ ,  $a(C_R)$  is monotonically increasing with  $C_R$ . At  $C_R = C_L = 1/2$ , we recover the result of the rotator model, i.e.  $a(1/2) = b(1/2) = 1/2$ . In fact,  $a(C_R)$  can be fitted very well to a parabola (Fig. 16) except at  $C_R = 0$  and  $C_R = 1$ , where  $N_1 = N = 1$  and  $N_2 = 0$  indicating a discontinuous transition at these two limits.

The scaling behavior for  $S=N$  can be derived from the relation  $N_1 + N_2 = N$ ,  $N_1 + 2N_2 = S$ , and Eq. (17),

$$\left\langle \frac{S}{N} \left[ 1 + b(C_R) \right] \right\rangle \propto N^{-0.57} \quad (18)$$

This scaling behavior is the same as that found for the fully occupied rotator model, Eq. (9), except that the asymptotic value, is now a function of  $C_R$ , rather than a single value 3=2, as for the rotator model.

As we mentioned before, each mirror on a given trajectory can be replaced by an appropriately chosen rotator to reproduce the same trajectory. After this operation, one can see that all right rotators are either on the outer side or on the inner side of the trajectory depending on the velocity direction of the particle, the same feature we found for the rotator model on a fully occupied lattice. We will refer to this rotator model generated from the mirror model as a quasi-rotator model. It is natural to study, in the same way as for the rotator model, the scaling behavior of the number of right rotators  $N_R$  and left rotators  $N_L$  on the trajectories for the quasi-rotator model. Our numerical results indicate the same power law behavior is obtained as in the rotator model, even when  $C_R \neq C_L$  where the rotator model and the quasi-rotator (or mirror model) cannot be mapped onto each other, (Fig. 17).

$$\left\langle \frac{N_R}{N} \frac{1}{2} \right\rangle_c = \left\langle \frac{N_L}{N} \frac{1}{2} \right\rangle_{cc} \propto N^{-0.57} \quad (19)$$

The asymptotic values for  $N_R=N$  and  $N_L=N$  are equal and the same as for the rotator model on the fully occupied lattice. This is not surprising, because  $N_R$  is associated with the outer side of a trajectory, while  $N_L$  is associated with the inner side of a trajectory (Fig. 3b). Although the mirror model for all  $C = 1$  corresponds to a quasi-rotator model, it is not clear how the quasi-rotator model can be generated directly, other than deriving it from a mirror model.

### 3.2 The partially occupied lattice

Here we only give a very brief discussion of the mirror model on a partially occupied square lattice. Again, this model can not be mapped onto a percolation model due to the fact that trajectories can cross themselves (Fig 2b). At  $C_R = C_L = C_E = 1/3$ , the mirror model can be mapped onto a growing self-avoiding walk trail introduced by Lyklem a<sup>(21)</sup> some time ago. Previous studies have shown that the distribution of the size of closed trajectories and the fractal dimension of large trajectories are drastically changed as soon as  $C < 1/3$  and  $d_f = 2$ , with logarithmic corrections<sup>(4,7,22,23)</sup>, indicating a first order phase transition. It has also been shown by numerical simulations that the moving particle exhibits super-diffusive behavior<sup>(7,23)</sup>, i.e. the diffusion constant increases with time logarithmically, suggesting that the hyperscaling relation  $1 = 2-d_f$  needs logarithmic corrections. It is not difficult to show that no "resector" can be formed in this model and consequently, that each site on a trajectory can only belong to either  $N_1$  or  $N_2$ .

## 4 Critical behavior of the rotator and the mirror model on the triangular lattice

### 4.1 The fully occupied lattice

In order to investigate the universality of the trajectory scaling behavior found on the square lattice, we also studied the triangular lattice. Similar to the rotator and mirror model on the square lattice, fixed rotators or fixed mirrors are randomly placed on the sites of the triangular lattice. The particle moves in six directions along the bonds of the lattice and its velocity is rotated by scatterers over an angle of  $\pi/3$  upon each collision, (Fig. 18). Since both the mirror model and the rotator model are discussed in this section, in order to avoid confusion, we define  $C_R^{\text{rotator}}$  and  $C_L^{\text{rotator}}$  as the concentration for right

rotators and left rotators, respectively, while we define  $C_R^{\text{mirror}}$  and  $C_L^{\text{mirror}}$  as the concentration for right mirror and left mirror, respectively. Similarly as before,  $C$  represents the total concentration of the scatterers.

For  $C = 1$ , earlier papers have shown<sup>(3,7)</sup> that the mirror model and the rotator model can be mapped into each other by replacing all the right (left) mirror on the trajectories by either right (left) rotators or left (right) rotators, respectively, provided  $C_R^{\text{rotator}} = C_R^{\text{mirror}}$  and  $C_L^{\text{rotator}} = C_L^{\text{mirror}}$ . Note that this is a global transformation rather than a local transformation, as was the case with the mapping of the rotator model onto the mirror model on the square lattice for  $C_R = C_L = 1/2$  (Fig. 19). In other words, the mirror model and the rotator model are equivalent. Again it can be shown that the trajectories cannot cross themselves and that all right rotators are either on the outer side or the inner side of the trajectories, depending on the direction in which the particle trajectory closes.

Both the mirror model and the rotator model can be mapped onto a site percolation rather than a bond percolation problem, as was the case for the rotator and the mirror models on the square lattice. For site percolation on the triangular lattice, the critical probability  $p_c$  to occupied a lattice site is  $1/2$ , so that the critical point occurs for  $C_L^{\text{mirror}} = C_R^{\text{mirror}} = C_L^{\text{rotator}} = C_R^{\text{rotator}} = 1/2$ . Here, we will only consider the rotator model, since the mirror model can be done in the same fashion. The number of right rotators  $N_R$  and left rotators  $N_L$  contained in the closed trajectories, exhibit the same power law behavior as on the square lattice, (Fig. 20),

$$\langle \frac{N_R}{N} - \frac{1}{2} \rangle_c = \langle \frac{1}{2} - \frac{N_L}{N} \rangle_c \propto N^{-0.57} \quad (20)$$

where  $N = N_R + N_L$ . The average is taken over all trajectories which contain  $N$  sites.

For the triangular lattice, the maximum number of times a site on a trajectory can be visited by the moving particle is three. This can be shown

by considering again the winding angle  $W$ . Upon each collision  $W$  will either increase or decrease by  $2\pi/3$ . Therefore, when the particle returns to the same site, the winding angle will be a multiple of  $2\pi/3$ . However, there are only three allowed angles of the form  $2n\pi/3$  on the triangular lattice, where  $n$  can be 0, 1 or 2, so that the maximum number of times a site be visited by the moving particle is indeed three. We define,  $N_1$ ,  $N_2$  and  $N_3$  as the number of sites visited by the particle once, twice, three times and four times, respectively, while  $S$  is the length of the trajectory. These quantities satisfy the following two sum rules,

$$N_1 + N_2 + N_3 = N \quad (21)$$

and

$$N_1 + 2N_2 + 3N_3 = S \quad (22)$$

The scaling behavior of  $N_1=N$ ,  $N_2=N$  and  $N_3=N$  is very similar to that found on the square lattice (Fig. 21),

$$\left\langle \frac{N_1}{N} \right\rangle \propto K_1 \quad \left\langle \frac{N_2}{N} \right\rangle \propto K_2 \quad \left\langle \frac{N_3}{N} \right\rangle \propto K_3 \quad N^{-0.57} \quad (23)$$

where  $K_1 = 0.3197$ ,  $K_2 = 0.4052$ ,  $K_3 = 0.2751$ . The sum of  $K_1$ ,  $K_2$  and  $K_3$  is one as required by Eq. (21). Although all values of  $K_i$  ( $i = 1, 2, 3$ ) are close to 1/3, they are not equal. Since each site has six adjacent bonds, the sites that belong to  $N_1$  and  $N_2$  form the "surface" of the trajectories, while the other sites that belong to  $N_3$  form the "bulk" of the trajectories. From Eq. (23), we see that the "surface" is much bigger than the "bulk". The asymptotic scaling behavior for  $S=N$  follows from Eq. (21), Eq. (22) and Eq. (23), to be,

$$\left\langle S \right\rangle \propto N^{1.9554} \quad N^{-0.57} \quad (24)$$

## 4.2 The partially occupied lattice

For the partially occupied lattice, i.e.  $C < 1$ , the rotator model and the mirror model can still be mapped into each other by a global transformation. That is, for a given trajectory, all left (right) mirrors on the trajectories can be replaced by either left (right) rotators or right (left) rotators respectively while empty sites remain empty, (Fig. 22). However, neither of the two models can be mapped onto a percolation problem, because the trajectories can cross themselves via the empty sites and consequently, the inner side and the outer side of large trajectories cannot be defined properly anymore, as was also the case for the square lattice partially occupied by scatterers. Nevertheless it was found numerically by Cohen and Wang<sup>(7)</sup> that for  $C < 1$ , there exists a linear critical line  $C_R = C_L = C=2$  (Fig. 23) and the cluster perimeter distribution exponent  $\gamma = 15/7$  and the fractal dimension  $d_f = 7/4$  of the trajectories along this critical line belong to the same universality class as that of site percolation. However, the existence of this simple critical line at low concentrations could not be established due to the prohibitively long numerical calculations needed. The lowest concentration studied in our simulations was  $C_R = C_L = C=2 = 0.225$ .

Since the trajectories can cross themselves, the winding angle  $W$  for closed trajectories is no more restricted to  $2\pi$  or  $-2\pi$ , so that it is natural to study the scaling behavior of  $W$ . Our numerical results (Fig. 24) for  $C_R = C_L = C=2 = 0.45$  show the following relation,

$$\langle \frac{W(N)}{N} \rangle \sim N^{-0.50} \quad (25)$$

in contrast to the stretched exponential behavior for the partially occupied rotator on the square lattice, Eq. (10). The asymptotic value for  $W(N) \sim N$  is zero, because the moving particle has equal probability to turn to its right or to its left.

For  $N_R$ ,  $N_L$  and  $N_E$ , our numerical simulations yield a different scaling exponent from that for the fully occupied lattice, (Fig. 25),

$$\langle \frac{N_R}{N} C_R \rangle < \frac{N_L}{N} C_L \rangle < \frac{N_E}{N} C_E \rangle \sim N^{-0.50} \quad (26)$$

This scaling behavior is the same as that of the partially occupied square lattice, Eq. (11). The exponent 0.50 can be understood in the same way as for the mirror model for  $C = 1$ .

Using the same kind of argument, as we used above for the fully occupied lattice, i.e. considering the change of the winding angle, we can show that the maximum number that a site on a trajectory can be visited by the moving particle is three. Unlike the rotator model on the partially occupied square lattice, Eq. (14), we find, that  $N_1=N$ ,  $N_2=N$  and  $N_3=N$  now follow the same scaling behavior along the critical line as the rotator model on the fully occupied lattice, (Fig. 26),

$$\langle \frac{N_1}{N} K_1 \rangle < \frac{N_2}{N} > < K_3 \rangle \sim N^{-0.57} \quad (27)$$

where  $K_1$ ,  $K_2$ ,  $K_3$  are functions of the concentration, which sum to 1, while the exponent 0.57 is independent of the concentration. Our numerical simulations also show that  $K_1$  is not a monotonic function of  $C$  while  $K_2$  is an increasing function of  $C$  and  $K_3$  is a decreasing function of  $C$ . However, all  $K_i$  ( $i = 1, 2, 3$ ) appear to converge to three different constants as  $C$  decreases, (Fig. 27).

## 5 Conclusion

In this paper, we have given, a more detailed numerical analysis than before of the nature of the trajectories generated in a Lorentz lattice gas model on both the square lattice and the triangular lattice at criticality. Our study has shown that the "structural" properties of these trajectories are highly non-trivial and yield some new universal scaling behavior probably related to the

scaling function exponent , in addition to that associated with the critical exponents and  $d_f$  found before. We hope that this study can lead to a more complete understanding of the complicated trajectories generated by a particle moving through randomly distributed scatterers on a lattice. The results are summarized in table I, table II and table III.

Our study only answered a few questions, but raised many more questions, as yet unanswered, among which we note the following.

1. For  $C = 1$ , why are the asymptotic values of  $N_R$  and  $N_L$  as well as of  $N_1$  and  $N_2$  on the fully occupied square lattice equal to  $N=2$ , i.e. why is  $K_1 = K_2 = 1/2$ ? What determines the asymptotic values for  $K_1, K_2$  and  $K_3$  on the fully occupied triangular lattice?
2. Our numerical simulations indicate that the  $K_i$  ( $i$  can be as large as 4 for the rotator model on the partially occupied square lattice and 3 for the triangular lattice) approach constants, as  $C$  is decreased along the critical line; in other words, the structure of the large trajectories hardly changes as the concentration of the scatterers is reduced, but why?
3. Although we have given an argument why the exponents describing the fluctuations of  $N_R = N$  along the critical line,  $C = 1$  for the mirror model, are all equal to 0.50, the more fundamental exponent 0.57 still remains elusive. We conjecture that the exact value is  $1 = 4/7$ , but it is not clear how to obtain this from theory.
4. Why does the winding angle  $W$  on the rotator model on the partially occupied square lattice exhibit a stretched exponential law behavior, while it exhibits a simple power law behavior on the partially occupied triangular lattice?
5. We find, that the  $N_i = N$  approach their asymptotic values  $K_i$  with a power law  $N^{-0.57}$  in all cases, except for the rotator model on the partially occupied square lattice where the exponent has a significantly different value, 0.39.

What is the origin of this difference? In the next paper, dealing with scaling behavior near criticality, we will show that  $\nu$  has the same value 3/7 in all cases except again for the partially occupied rotator model on the square lattice. This may indicate that the scaling behavior of the  $N \times N$  and the exponent are related to each other.

6. How can one understand the difference between the phase diagram of the partially occupied rotator model on the square lattice and that on the triangular lattice? Do the "re-actors" play an important role here?

7. How are the lattice sites visited by a moving particle, once, twice, etc. correlated to each other on the lattice, with respect to both space and time?

#### Acknowledgment

The authors are grateful to J. Machta and F. Wang for useful discussions, and R. Zi for a number of helpful comments on the manuscript. This work is supported under grant DE-FG 02-88ER 13847 of the Department of Energy.

## References

1. Th. W. Ruijgrok and E. G. D. Cohen, *Phys. Lett. A* **133**, 415 (1988).
2. X. P. Kong and E. G. D. Cohen, *Phys. Rev. B* **40**, 4838 (1989).
3. X. P. Kong and E. G. D. Cohen, *J. Stat. Phys.* **62**, 737 (1991).
4. R. M. Zi, X. P. Kong and E. G. D. Cohen, *Phys. Rev. B* **44**, 2410 (1991).
5. E. G. D. Cohen, New types of diffusion in lattice gas cellular automata, in *Microscopic Simulations of Complex Hydrodynamic Phenomena*, M. Mareschal and B. L. Holian, eds. (Plenum Press, New York, 1992), p. 137.
6. H. F. Meng and E. G. D. Cohen, *Phys. Rev. E* **50**, 2482 (1994).
7. E. G. D. Cohen and F. Wang, *J. Stat. Phys.* **81**, 445 (1995).
8. F. Wang and E. G. D. Cohen, *J. Stat. Phys.* **81**, 467 (1995).
9. E. G. D. Cohen and F. Wang, *Physica A* **219**, 56 (1995).
10. E. G. D. Cohen and F. Wang, *Fields Institute Communications*, **6**, 43 (1996).
11. B. Sapoval, M. Rosso and J. F. Gouyet, *J. Phys. Lett. (Paris)* **46**, L149 (1985).
12. R. M. Zi, *Phys. Rev. Lett.* **56**, 545 (1986).
13. H. Saleur and B. Duplantier, *Phys. Rev. Lett.* **58**, 2325 (1987).
14. R. M. Zi, P. T. Cummings, and G. Stell, *J. Phys. A* **17**, 3009 (1984).
15. J. Gunn and M. Ortuno, *J. Phys. A* **18**, 1035 (1985).
16. P. Grassberger, *J. Phys. A* **19**, 2675 (1986).
17. R. M. Zi. *Private Communication*.
18. M. Ortuno, J. Ruiz and M. F. Gunn, *J. Stat. Phys.* **65**, 453 (1991).
19. L. A. Bunimovich and S. E. Troubetzkoy, *J. Stat. Phys.* **74**, 1 (1994).
20. L. A. Bunimovich and S. E. Troubetzkoy, *J. Stat. Phys.* **67**, 289 (1992).
21. J. Lyklem, *J. Phys. A* **18**, L617 (1985).
22. R. M. Bradley, *Phys. Rev. B* **41**, 914 (1989).
23. A. L. Owczarek and T. P. Mallberg, *J. Stat. Phys.* **79**, 951 (1995).

### Figure Captions

Fig. 1. Scattering rules for the rotator model and the mirror model on the square lattice (a) right rotators; (b) left rotators; (c) right mirrors; (d) left mirrors.

Fig. 2. (a) a typical closed trajectory generated by a moving particle on the square lattice partially occupied by rotators. Here  $W = 6$ ,  $N_R = 10$ ,  $N_L = 2$ ,  $N_E = 7$ ,  $N_1 = 18$ ,  $N_2 = 1$ ,  $N_3 = 0$ ,  $N_4 = 0$ ,  $N = 19$  and  $S = 20$ . (b) The same trajectory generated by a moving particle on the square lattice partially occupied by mirrors. Here  $M_R = 8$  and  $M_L = 4$ .

Fig. 3. (a) A typical counter-clockwise closed trajectory on the square lattice. Note that all left rotators and all right rotators are on the outer side and inner side of the trajectory, respectively. Here  $W = 2$ ,  $N_R = 5$ ,  $N_L = 10$ ,  $N_1 = 14$ ,  $N_2 = 1$ ,  $N = 15$  and  $S = 16$ . (b) The same trajectory generated by mirrors on the square lattice. Mirrors (fat solid lines) on the outer side of the trajectory form a bond percolation cluster perimeter on one of the two sublattices (dashed lines), while mirrors on the inner side of the trajectory form a bond percolation cluster perimeter on the other sublattice (dotted lines). Here  $M_R = 6$  and  $M_L = 9$ .

Fig. 4. The probability density  $P(N_R = N)$  vs  $N_R = N$  for the rotator model. The data were obtained from trajectories consisting of 1300 to 1500 sites ( ) and 2000 to 2300 sites (+). (a) both clockwise and counter-clockwise trajectories are included in the data. The solid and the dashed curves are described by the double Gaussians;  $23.7 e^{-7058(N_R = N - 0.5182)^2} + 23.7 e^{-7058(N_R = N + 0.5182)^2}$  and  $28.0 e^{-9856(N_R = N - 0.5145)^2} + 28.0 e^{-9856(N_R = N + 0.5145)^2}$ , respectively. (b) only the clockwise trajectories are included in the data. The solid and the dashed curves are described by the Gaussians,  $23.7 e^{-7058(N_R = N - 0.5182)^2}$  and  $28.0 e^{-9856(N_R = N - 0.5145)^2}$ , respectively. For increasing values of  $N$  the curves become taller and narrower.

Fig. 5. Scaling behavior of  $N_R$  and  $N_L$  for clockwise and counter-clockwise

closed trajectories, respectively, on the square lattice fully occupied by rotators,  $C_R = C_L = 1/2$ :  $\log_2 < N_R = N_{1/2} >_c$  vs  $\log_2 S$  ( ),  $\log < N_L = N_{1/2} >_\infty$  vs  $\log_2 S$  (+). The slope of the lines through both sets of points is 0.57.

Fig. 6. Scaling behavior of  $N_1$  and  $N_2$  for trajectories on the square lattice fully occupied by rotators,  $C_R = C_L = 1/2$ :  $\log_2 < N_1 = N_{1/2} >$  vs  $\log_2 S$  ( ). Also plotted is  $\log < 1/2 < N_2 = N > >$  vs  $\log_2 S$  (+), which have the same values. The slope of the lines through both sets of points is 0.57.

Fig. 7. Schematic phase diagram for the rotator model on the square lattice. The inner solid line extends to  $C = 0.65$  and is tangent to the line  $C = 1$ , the dashed line is conjectured.

Fig. 8. Scaling behavior of the winding  $W$  for trajectories on the square lattice partially occupied by rotators, for a typical concentration  $C = 0.9$  with  $C_R = 0.477$ ,  $C_L = 0.423$ :  $< W = N_{(C_R - C_L)/2} >$  vs  $\log_2 S$  ( ). The solid curve is described by  $(C_R - C_L) + 7.5 \cdot 2^{(2.80 S^{0.18})}$ .

Fig. 9. Scaling behavior of  $N_R$ ,  $N_L$  and  $N_E$  for trajectories on the square lattice partially occupied by rotators, for  $C = 0.9$  with  $C_R = 0.477$ ,  $C_L = 0.423$ ,  $C_E = 0.1$ :  $\log_2 < N_R = N_{(C_R)} >$  vs  $\log_2 S$  ( ),  $\log < N_L = N_{(C_L)} >$  vs  $\log_2 S$  (+),  $\log_2 < N_E = N_{(C_E)} >$  vs  $\log_2 S$  (2). The slope of the lines through the points is 0.50.

Fig. 10. The two smallest "reectors", each of six sites with one empty site, forming a closed trajectory on the square lattice partially occupied by rotators. Note that neither of the two right rotators can be replaced by either a right mirror or a left mirror, so the "reector" cannot be formed in the mirror model. We also note that this reector is even smaller than that reported previously<sup>(9,10)</sup>.

Fig. 11. Scaling behavior of  $N_1$ ,  $N_2$ ,  $N_3$  and  $N_4$  for trajectories on the square lattice partially occupied by rotators, for  $C = 0.9$  with  $C_R = 0.477$ ,  $C_L =$

0.423,  $C_E = 0.1 : \log_2 \langle N_1 = N \rangle \leq K_1 \rangle \text{ vs } \log_2 S$  ( ),  $\log_2 \langle N_2 = N \rangle \leq K_2 \rangle \text{ vs } \log_2 S$  ( + ),  $\log_2 \langle N_3 = N \rangle \text{ vs } \log_2 S$  ( 2 ),  $\log_2 \langle N_4 = N \rangle \text{ vs } \log_2 S$  ( ), where the values of  $K_1$ ,  $K_2$ ,  $K_3$  and  $K_4$  are 0.3047, 0.2671, 0.2223 and 0.2056, respectively. The slope of the lines through the points is 0.39.

Fig. 12. Values of  $K_1$  ( ),  $K_2$  ( + ),  $K_3$  ( 2 ) and  $K_4$  ( ) for trajectories on the square lattice partially occupied by rotators as a function of  $C$ . The lines through the points are drawn to guide the eye.

Fig. 13. The probability density  $P(M_R = N)$  vs  $M_R = N$  for the mirror model on the fully occupied square lattice. The data were obtained from trajectories consisting of 1300 to 1500 sites ( ) and 2000 to 2300 sites ( + ). The solid and the dashed curves are described by the Gaussians;  $31e^{-2950(M_R = N - 0.4)^2}$  and  $39e^{-4950(M_R = N - 0.4)^2}$ , respectively.

Fig. 14. Scaling behavior of  $M_R$  for trajectories on the square lattice fully occupied by m irors at di erent  $C_R$ :  $\log_2 \langle M_R = N \rangle \leq C_R \rangle \text{ vs } \log_2 S$ ,  $C_R = 0.1$  ( ),  $C_R = 0.2$  ( + ),  $C_R = 0.3$  ( 2 ),  $C_R = 0.4$  ( ). The slope of the lines through the points is 0.50.

Fig. 15. Scaling behavior of  $N_1$  for trajectories on the square lattice by m irors at di erent  $C_R$  along the critical line  $C = 1 : \log_2 \langle N_1 = N \rangle \text{ a}(C_R) \rangle \text{ vs } \log_2 S$ ,  $C_R = 0.1$  ( ),  $C_R = 0.2$  ( + ),  $C_R = 0.3$  ( 2 ),  $C_R = 0.4$  ( ). The slope of the lines through the points is 0.50.

Fig. 16. For the mirror model on the fully occupied square lattice,  $a(C_R)$  vs  $C_R$  ( ),  $b(C_R)$  vs  $C_R$  ( + ). The solid line and the dashed line are described by  $0.5 + 0.59(0.25 - C_R C_L)$  and  $0.5 - 0.59(0.25 - C_R C_L)$ , respectively.

Fig. 17. Scaling behavior of  $N_R$  for trajectories on the square lattice fully occupied by rotators mapped from m irors, ie. for the quasi-rotator model, at di erent  $C_R$ :  $\log_2 \langle N_R = N \rangle \text{ vs } \log_2 S$ ,  $C_R = 0.4$  ( ),  $C_R = 0.3$  ( + ),  $C_R = 0.2$  ( 2 ),  $C_R = 0.1$  ( ). The slope of the lines through the points is 0.57.

Fig. 18. Scattering rules for the mirror and the rotator models on the triangular lattice. (a) the six velocity directions; (b) rotator scatterers; (c) mirror scatterers.

Fig. 19. (a) A typical clockwise closed trajectory on the triangular lattice. All right rotators and all left rotators are on the outer side and on the inner side of the trajectory respectively and form two site percolation cluster perimeters on the triangular lattice. Here  $N_1 = 9$ ,  $N_2 = 3$ ,  $N_3 = 6$ ,  $N_R = 13$ ,  $N_L = 5$ ,  $N = 18$ , and  $S = 33$ . (b) the same trajectory generated by mirror models on the same lattice. Note all right rotators have been replaced by right mirror models while all left rotators have been replaced by left mirror models. Here  $M_R = N_R = 13$  and  $M_L = N_L = 5$ .

Fig. 20. Scaling behavior of  $N_R$  and  $N_L$  for trajectories on the triangular lattice fully occupied by rotators,  $C_R = C_L = 1/2$ :  $\log_2 < N_R = N >_{\text{c}}$  vs  $\log_2 S$  ( ),  $\log < N_L = N >_{\text{c}}$  vs  $\log_2 S$  (+). The slope of the lines through the points is 0.57.

Fig. 21. Scaling behavior of  $N_1$ ,  $N_2$  and  $N_3$  for trajectories on the triangular lattice fully occupied by rotators,  $C_R = C_L = 1/2$ :  $\log_2 < N_1 = N >_{\text{c}}$  vs  $\log_2 S$  ( ),  $\log < N_2 = N >_{\text{c}}$  vs  $\log_2 S$  (+).  $\log_2 < N_3 = N >_{\text{c}}$  vs  $\log_2 S$  (2), where the values of  $K_1$ ,  $K_2$  and  $K_3$  are 0.3197, 0.4052 and 0.2751 respectively. The slope of the fitting lines are 0.57.

Fig. 22. (a) A typical closed trajectory generated by a moving particle on the triangular lattice partially occupied by rotators. Note that the trajectory crosses itself. Here  $W = 0$ ,  $N_R = 3$ ,  $N_L = 3$ ,  $N_E = 5$ ,  $N_1 = 10$ ,  $N_2 = 1$ ,  $N_3 = 0$ ,  $N = 11$  and  $S = 12$ . (b) The same trajectory generated by a moving particle on the triangular lattice partially occupied by mirror models. Right rotators are replaced by right mirror models while left rotators are replaced by left mirror models. Here  $M_R = N_R = 3$  and  $M_L = N_L = 3$ .

Fig. 23. Phase diagram for both the mirror and the rotator models on the

triangular lattice. The solid critical line has been computed for  $C > 0.6$ , the dashed critical line is conjectured.

Fig. 24. Scaling behavior of  $W$  for trajectories on the triangular lattice partially occupied by rotators, for a typical concentration  $C = 0.8$  with  $C_R = C_L = 0.4$ :  $\log \langle N \rangle$  vs  $\log_2 S$  ( ). The slope of the line through the points is 0.50.

Fig. 25. Scaling behavior of  $N_R$ ,  $N_L$  and  $N_E$  for trajectories on the triangular lattice partially occupied by rotators, for  $C = 0.8$  with  $C_R = C_L = 0.4$  and  $C_E = 0.2$ :  $\log_2 \langle N_R \rangle$  vs  $\log_2 S$  ( ),  $\log \langle N_L \rangle$  vs  $\log_2 S$  (+),  $\log_2 \langle N_E \rangle$  vs  $\log_2 S$  (2). The slope of the lines through the points is 0.50.

Fig. 26. Scaling behavior of  $N_1$ ,  $N_2$  and  $N_3$  for trajectories on the triangular lattice partially occupied by rotators, for  $C = 0.8$  with  $C_R = C_L = 0.4$  and  $C_E = 0.2$ :  $\log_2 \langle N_1 \rangle$  vs  $\log_2 S$  ( ),  $\log \langle N_2 \rangle$  vs  $\log_2 S$  (+),  $\log_2 \langle N_3 \rangle$  vs  $\log_2 S$  (2), where the values of  $N_1$ ,  $N_2$  and  $N_3$  are 0.3356, 0.3391 and 0.3254, respectively. The slope of the lines through the points is 0.57.

Fig. 27. Values of  $K_1$  ( ),  $K_2$  (+) and  $K_3$  (2) for trajectories on the triangular lattice partially occupied by rotators as a function of  $C$ . The lines through the points are drawn to guide the eye.

TABLE I: Critical behavior for  $C = 1$ 

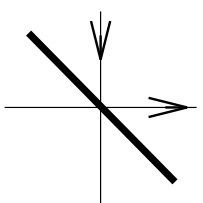
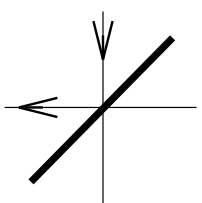
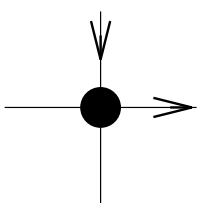
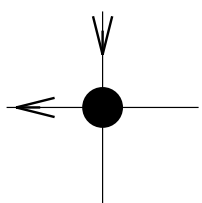
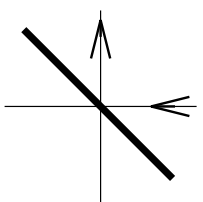
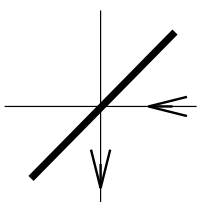
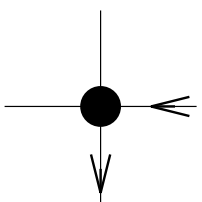
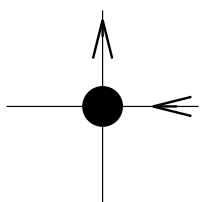
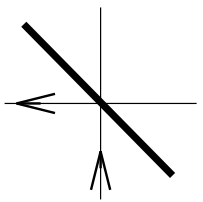
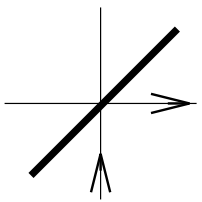
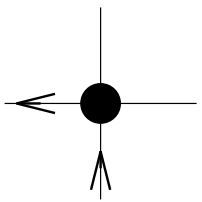
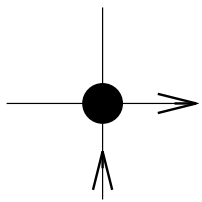
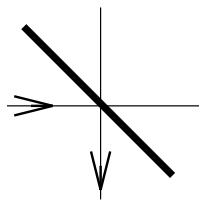
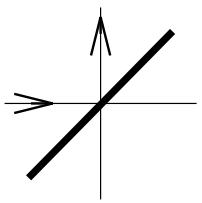
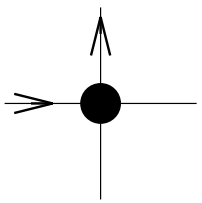
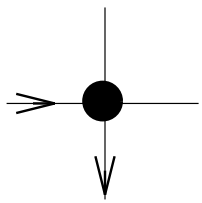
Square Lattice		Triangular Lattice
Rotator	$M_{\text{rror}}$	$M_{\text{rror}} = m_{\text{rror}}$
$\langle \frac{N_R}{N} \frac{1}{2} \rangle_c =$ $\langle \frac{N_L}{N} \frac{1}{2} \rangle_{cc} N^{0.57}$	$\langle \frac{M_R}{J_N} C_R j \rangle =$ $\langle \frac{M_L}{J_N} C_L j \rangle = N^{0.50}$	$\langle \frac{N_R}{N} \frac{1}{2} \rangle_c =$ $\langle \frac{N_L}{N} \frac{1}{2} \rangle_{cc} N^{0.57}$
$\langle \frac{N_1}{N} \frac{1}{2} \rangle =$ $\langle \frac{1}{2} \frac{N_2}{N} \rangle = N^{0.57}$	$\langle \frac{N_1}{N} a(C_R) \rangle =$ $\langle b(C_R) \frac{N_2}{N} \rangle = N^{0.57}$	$\langle \frac{N_1}{N} 0.3197 \rangle$ $\langle 0.4052 \frac{N_2}{N} \rangle$ $\langle 0.2751 \frac{N_3}{N} \rangle = N^{0.57}$
$\langle \frac{S}{N} \frac{3}{2} \rangle = N^{0.57}$	$\langle \frac{S}{N} 1 b(C_R) \rangle = N^{0.57}$	$\langle \frac{S}{N} 1.9554 \rangle = N^{0.57}$

TABLE II: Critical behavior for  $C = 0.9$ 

Square Lattice		Triangular Lattice
Rotator	Mirror	Rotator=mirror
$\langle \frac{W}{N} (C_R - C_L) j \rangle = 2^{-2.88^{0.18}}$		$\langle \frac{W}{N} j \rangle \sim N^{-0.50}$
$\langle \frac{N_R}{N} C_R j \rangle =$		$\langle \frac{N_R}{N} C_R j \rangle =$
$\langle \frac{N_L}{N} C_L j \rangle$		$\langle \frac{N_L}{N} C_L j \rangle$
$\langle \frac{N_E}{N} C_E j \rangle \sim N^{-0.50}$	Superdiffusion	$\langle \frac{N_E}{N} C_E j \rangle \sim N^{-0.50}$
$\langle \frac{N_1}{N} 0.2671 \rangle$	( $\epsilon = 1, d_f = 2$ )	$\langle \frac{N_1}{N} 0.3308 \rangle$
$\langle \frac{N_2}{N} 0.3047 \rangle$		$\langle 0.3669 \frac{N_2}{N} \rangle$
$\langle 0.2223 \frac{N_3}{N} \rangle$		$\langle 0.3023 \frac{N_3}{N} \rangle \sim N^{-0.57}$
$\langle 0.2059 \frac{N_4}{N} \rangle \sim N^{-0.39}$		
$\langle \frac{S}{N} 2.3670 \rangle \sim N^{-0.39}$		$\langle \frac{S}{N} 1.9715 \rangle \sim N^{-0.57}$

TABLE III: Critical behavior for  $C = 0.8$ 

Square Lattice		Triangular Lattice
Rotator	Mirror	Rotator=mirror
$\langle \frac{W}{N} (C_R - C_L) j \rangle \sim 2^{-1.48 \pm 0.18}$		$\langle \frac{W}{N} j \rangle \sim N^{-0.50}$
$\langle \frac{N_R}{N} C_R j \rangle =$		$\langle \frac{N_R}{N} C_R j \rangle =$
$\langle \frac{N_L}{N} C_L j \rangle$		$\langle \frac{N_L}{N} C_L j \rangle$
$\langle \frac{N_E}{N} C_E j \rangle \sim N^{-0.50}$	Superdiffusion	$\langle \frac{N_E}{N} C_E j \rangle \sim N^{-0.50}$
$\langle \frac{N_1}{N} 0.2680 \rangle$	( $\zeta = 1, d_f = 2$ )	$\langle \frac{N_1}{N} 0.3356 \rangle$
$\langle \frac{N_2}{N} 0.2760 \rangle$		$\langle 0.3391 \frac{N_2}{N} \rangle$
$\langle 0.2365 \frac{N_3}{N} \rangle$		$\langle 0.3254 \frac{N_3}{N} \rangle \sim N^{-0.57}$
$\langle 0.2195 \frac{N_4}{N} \rangle \sim N^{-0.39}$		
$\langle \frac{S}{N} 2.4075 \rangle \sim N^{-0.39}$		$\langle \frac{S}{N} 1.990 \rangle \sim N^{-0.57}$



(a)

(b)

(c)

(d)

Fig. 1

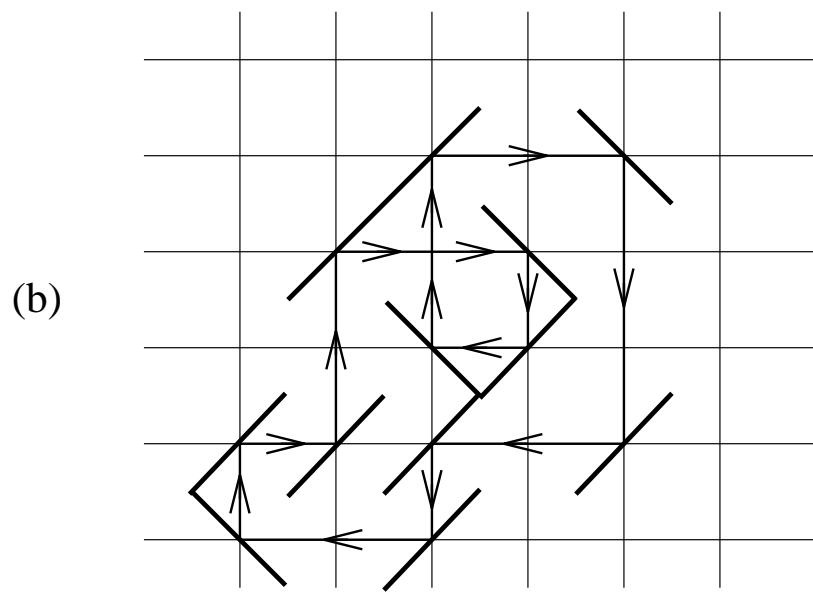
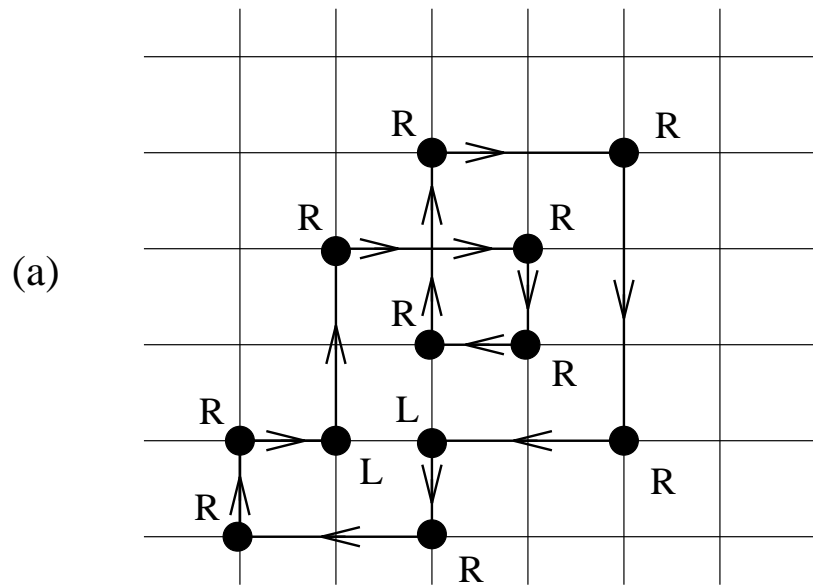


Fig. 2

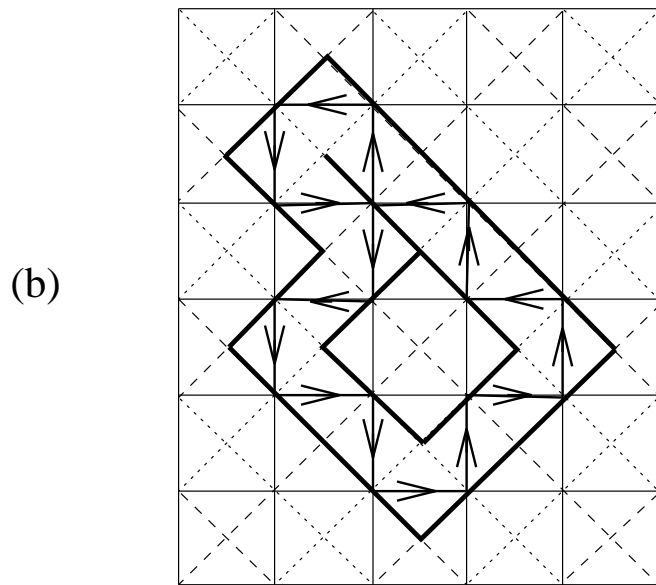
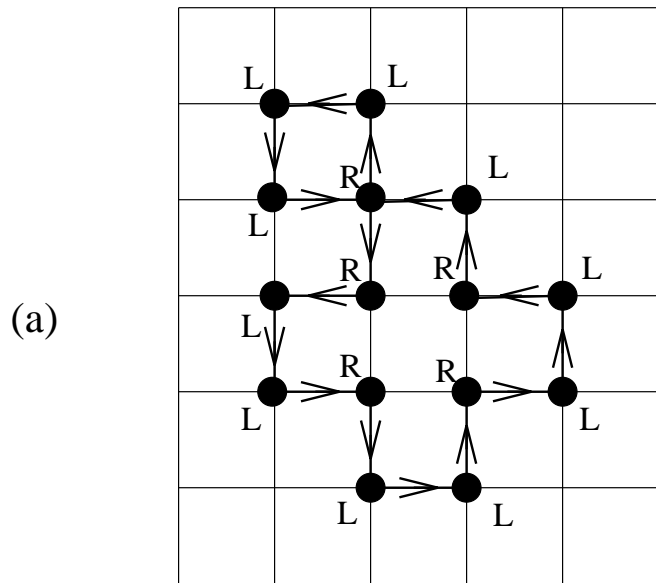
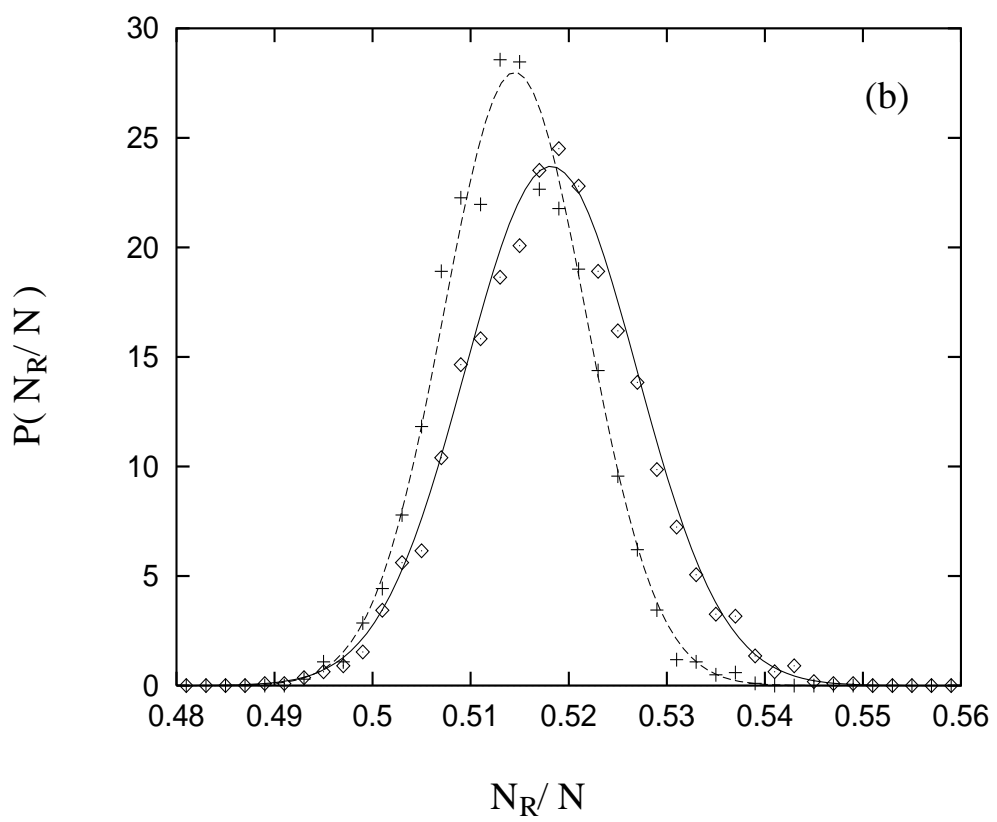
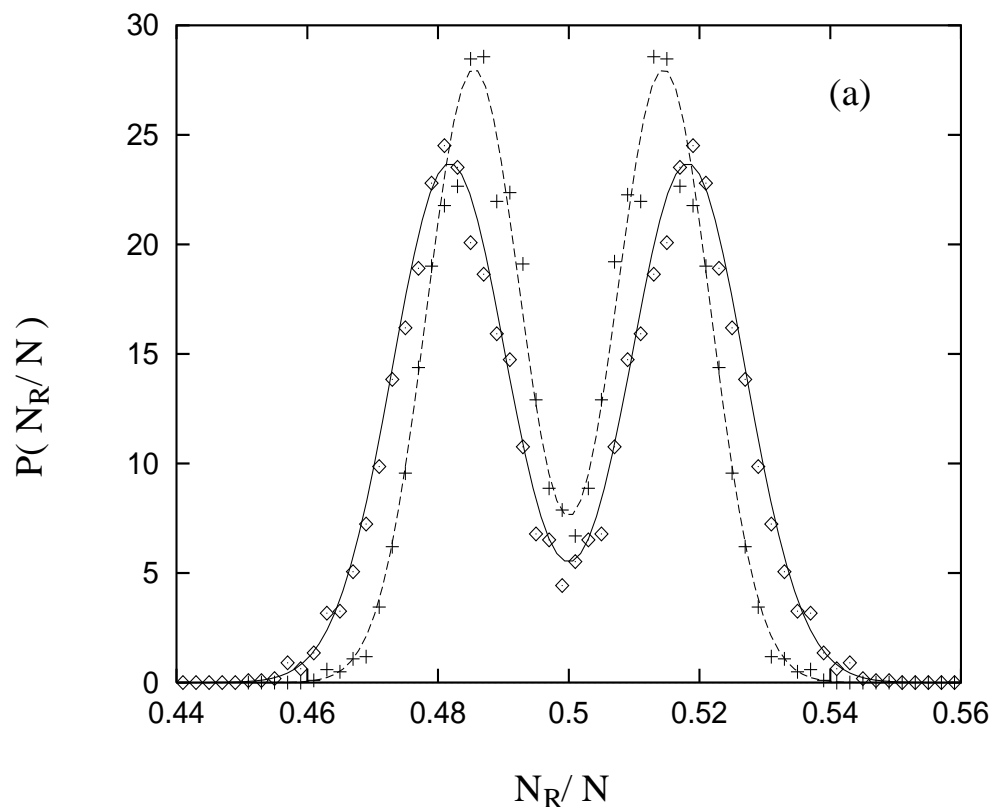


Fig. 3



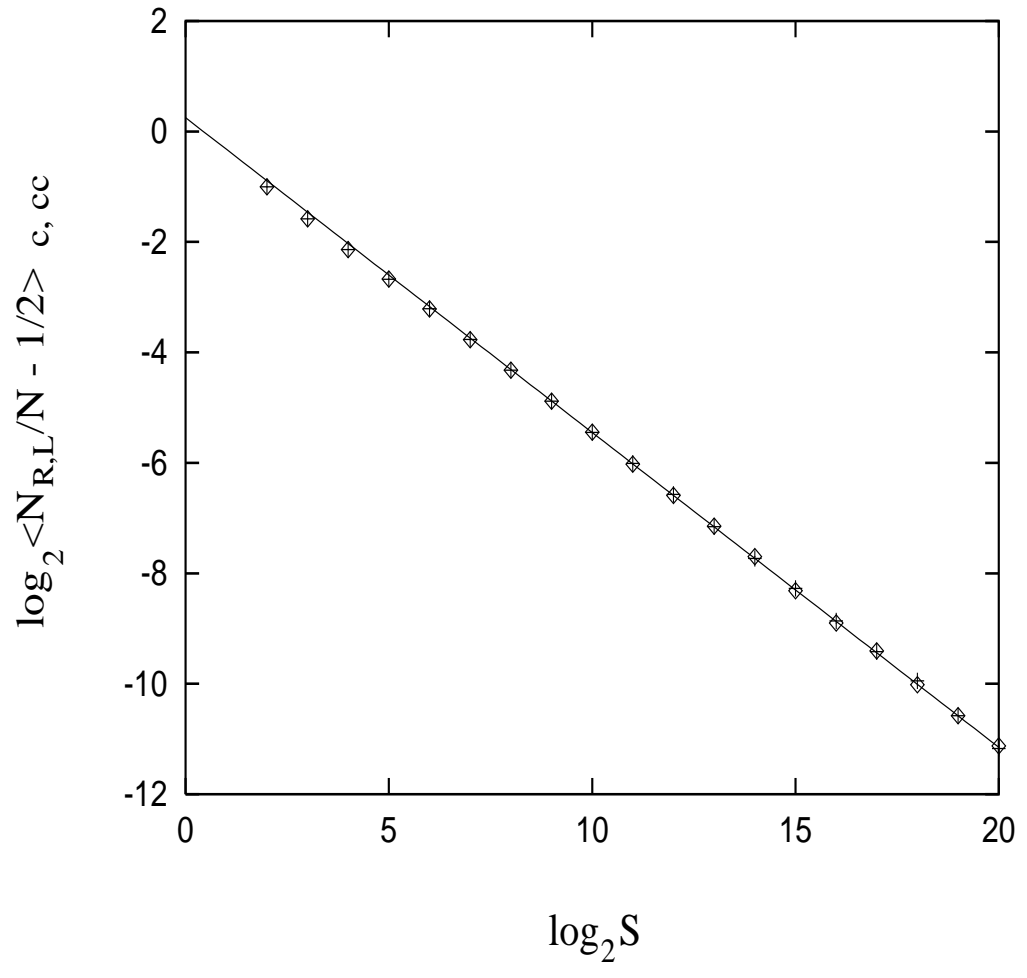


Fig. 5

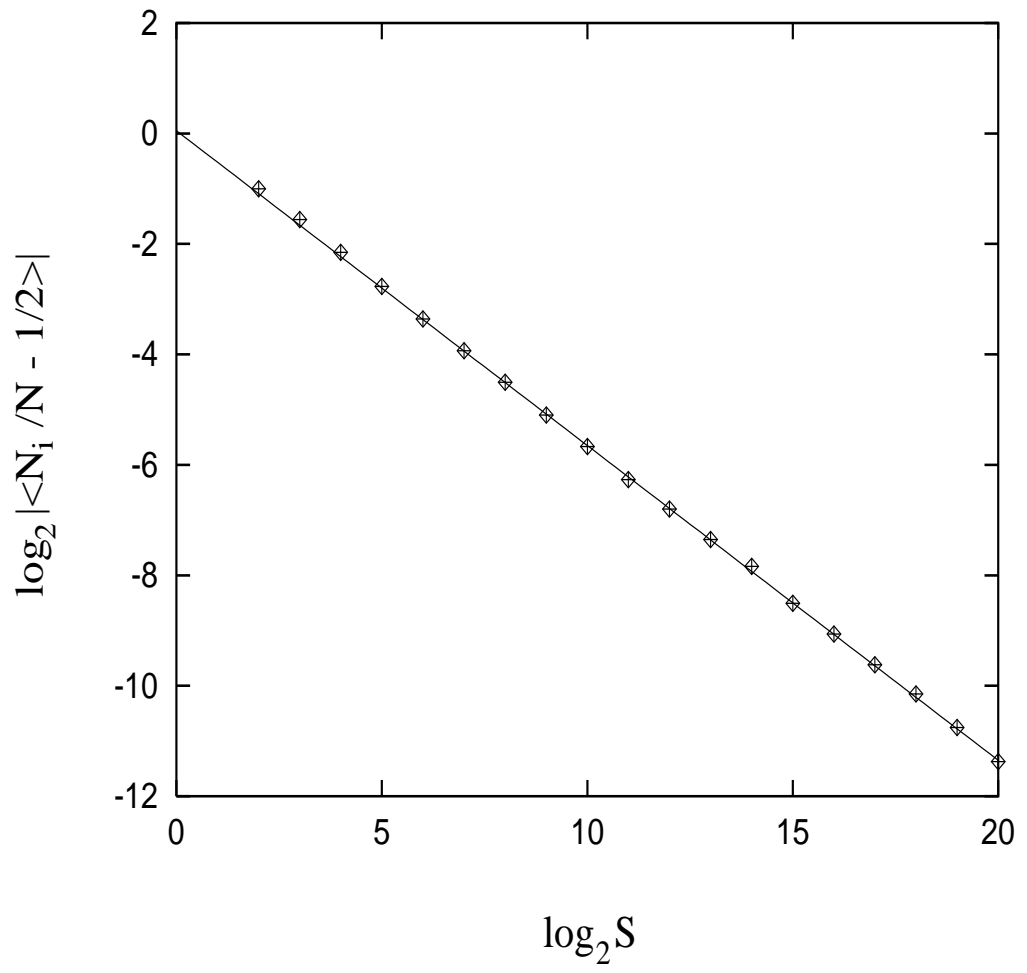


Fig. 6

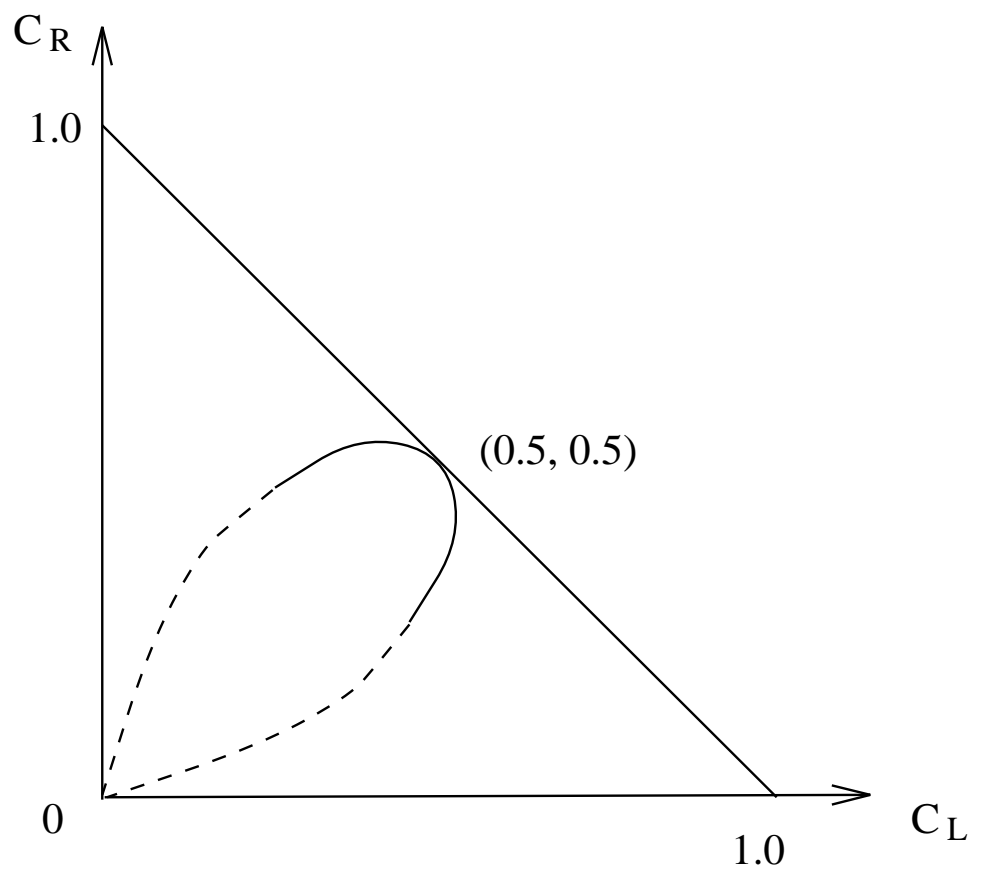


Fig. 7

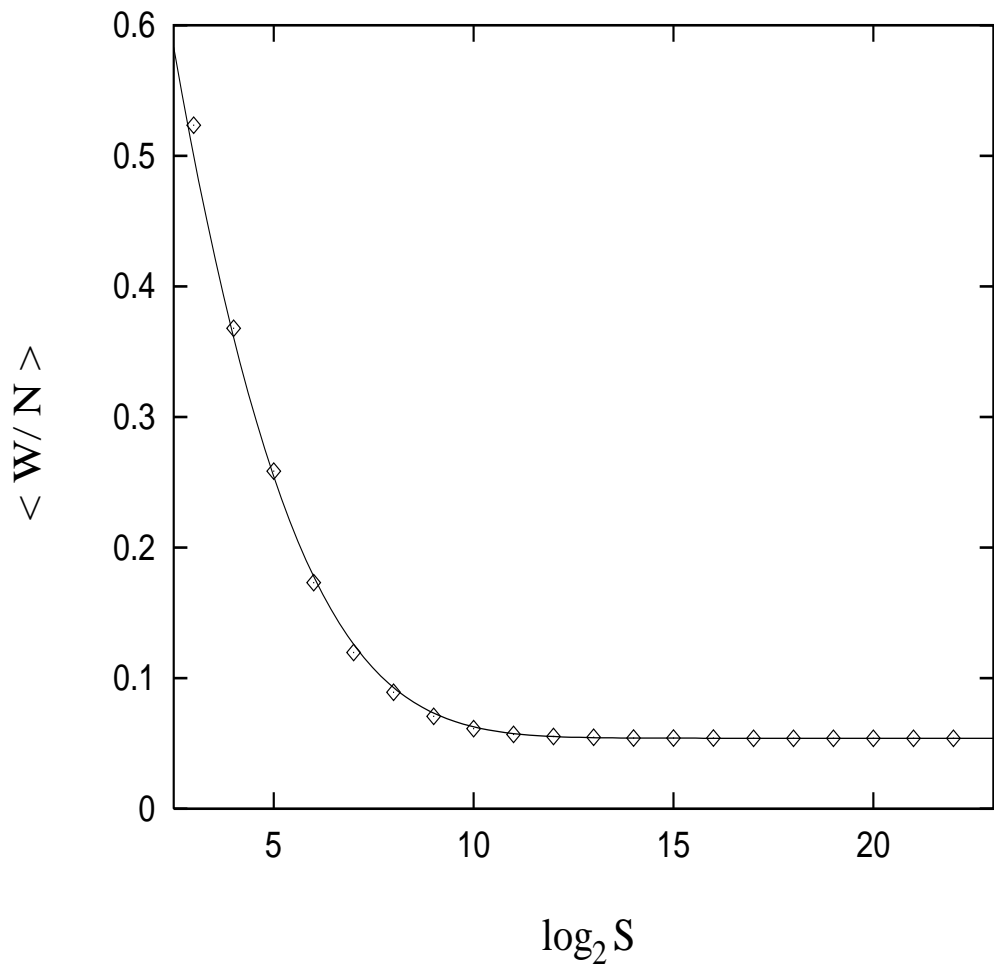


Fig. 8

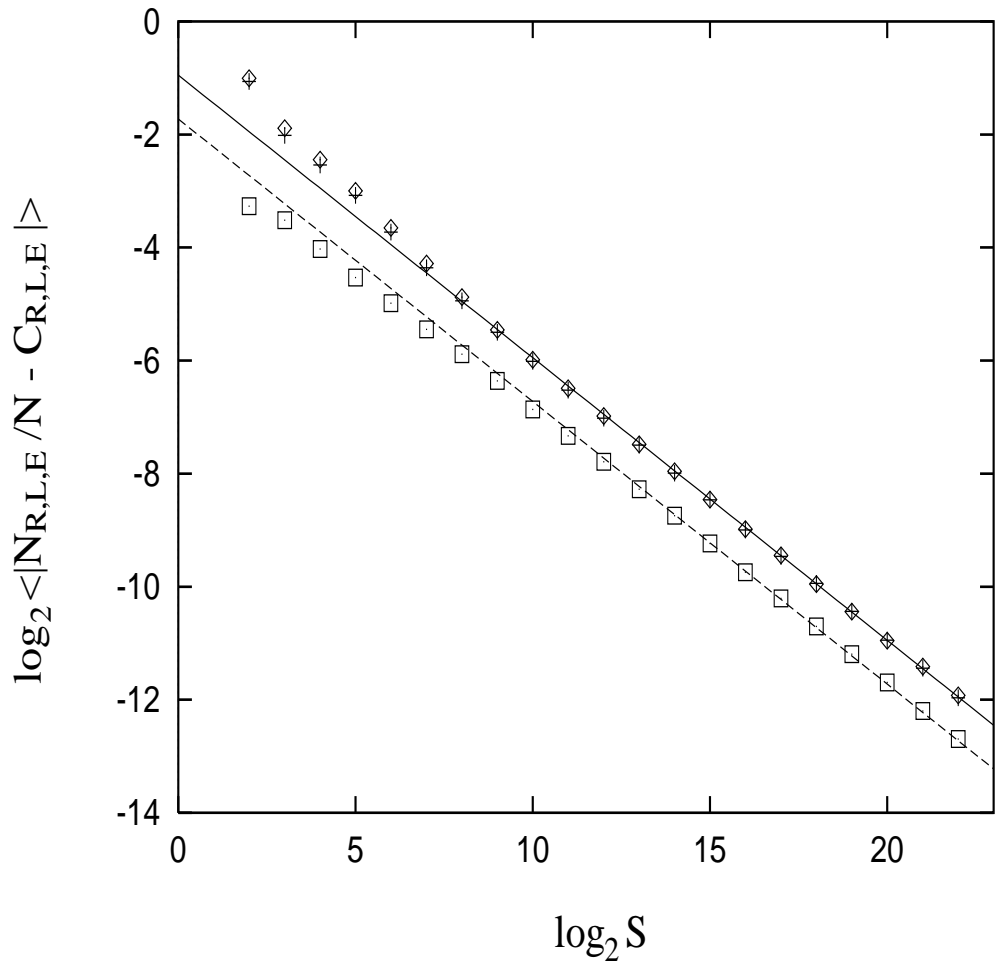


Fig. 9

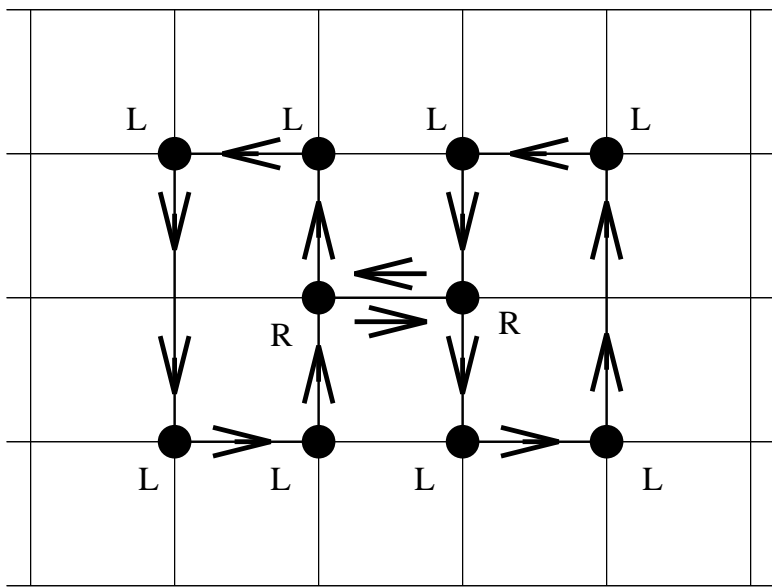


Fig. 10

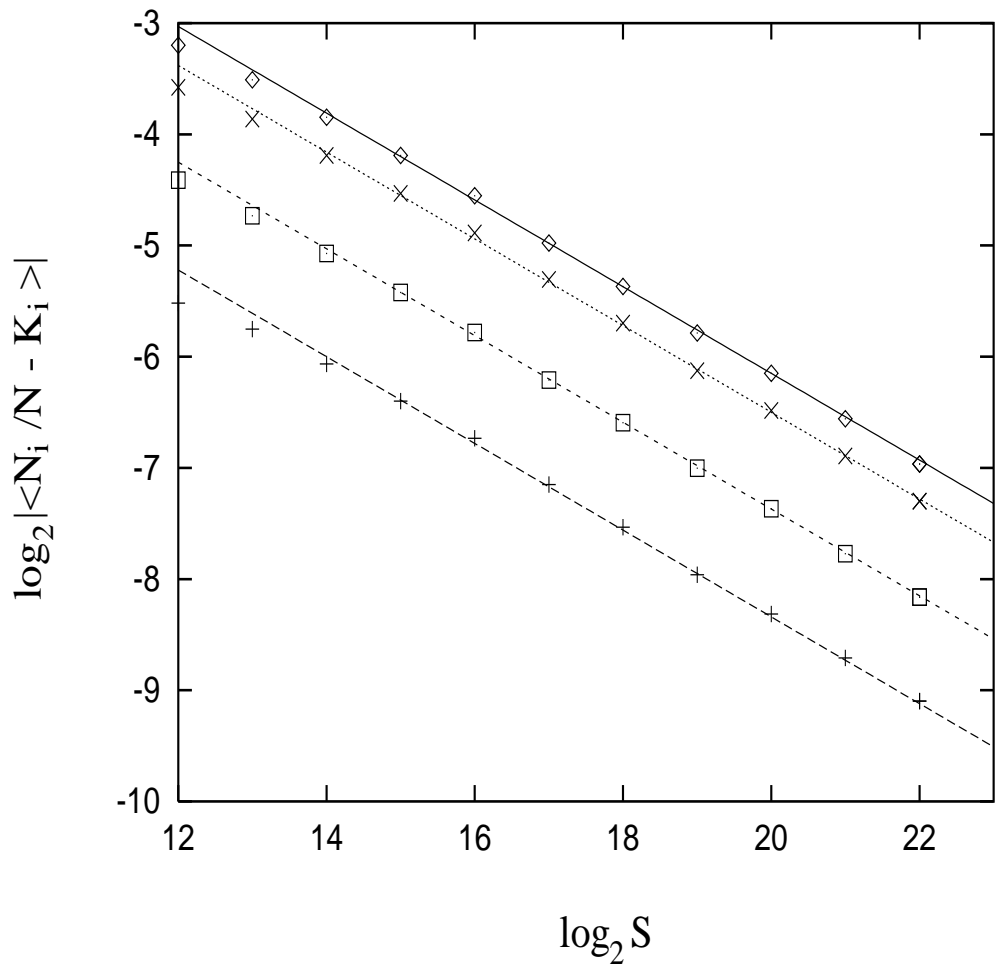


Fig. 11

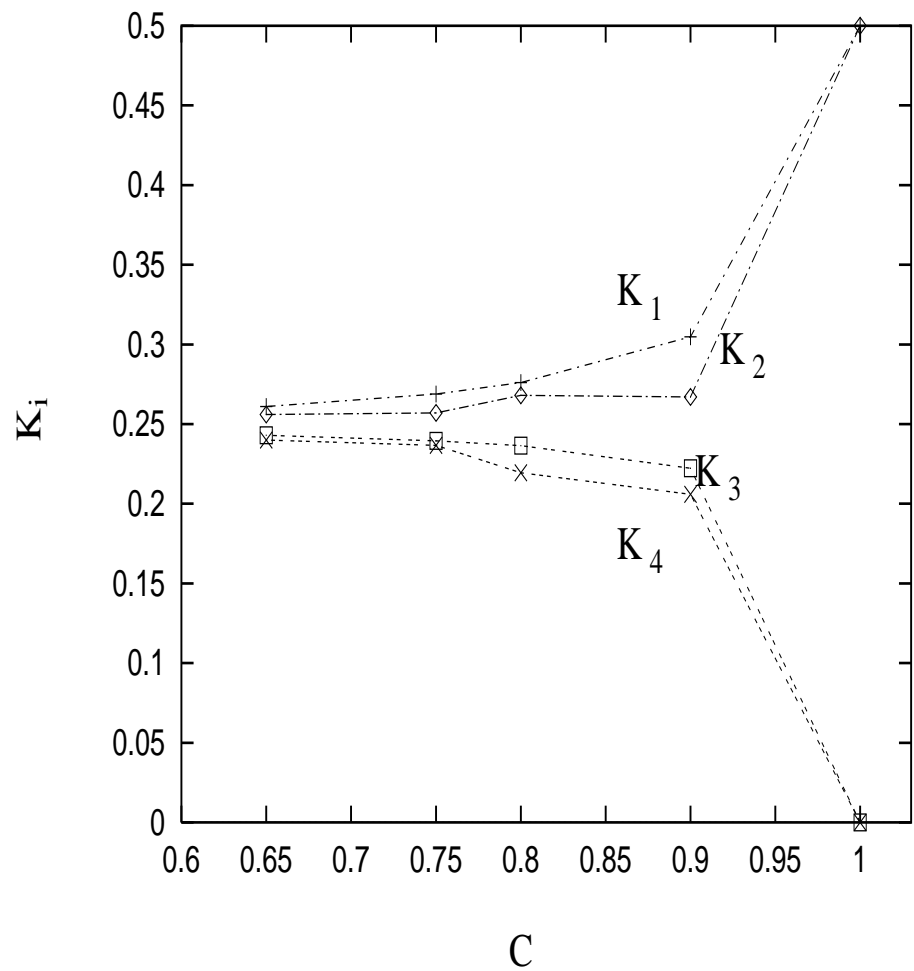


Fig. 12

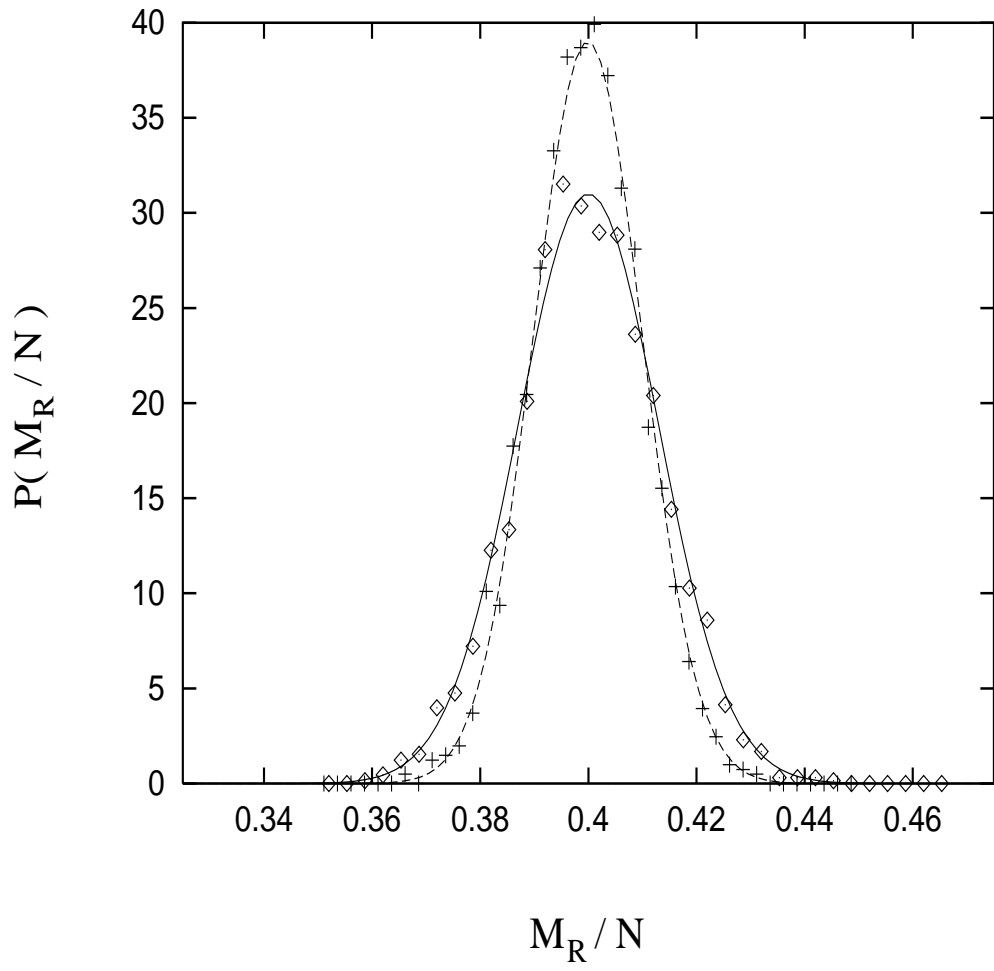


Fig. 13

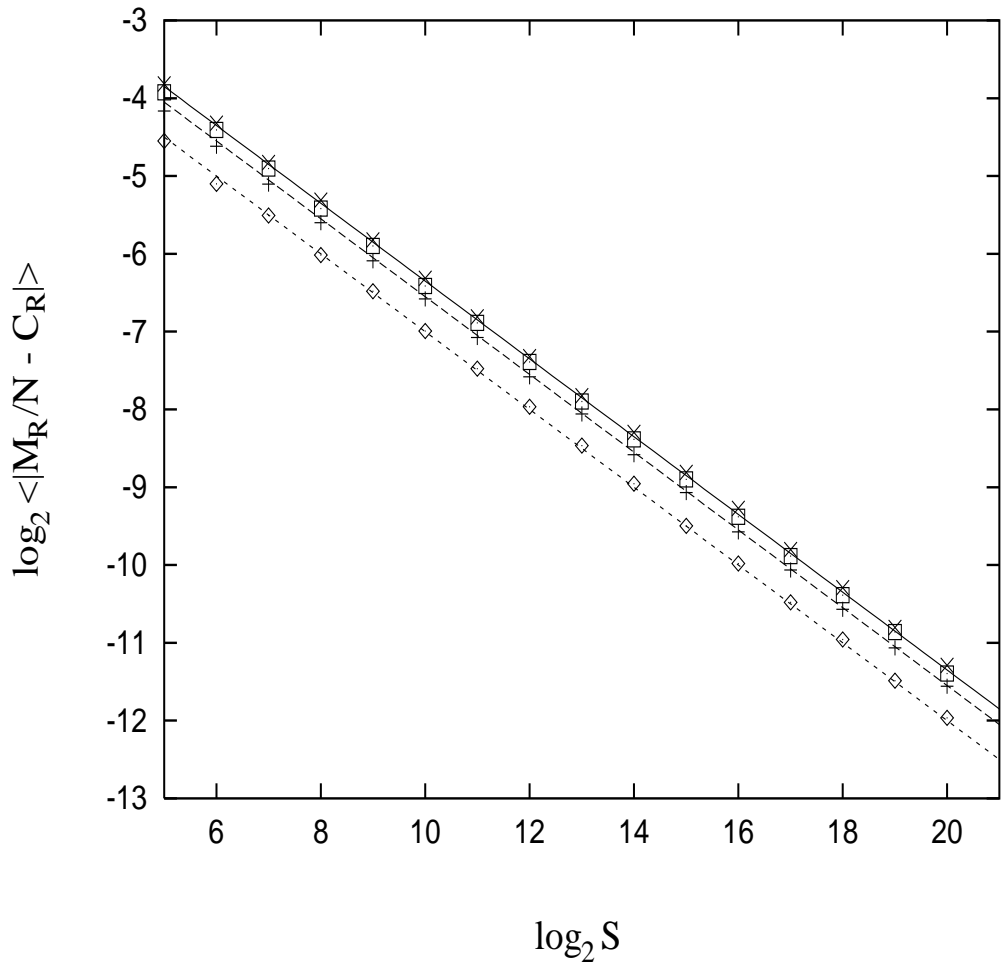


Fig. 14

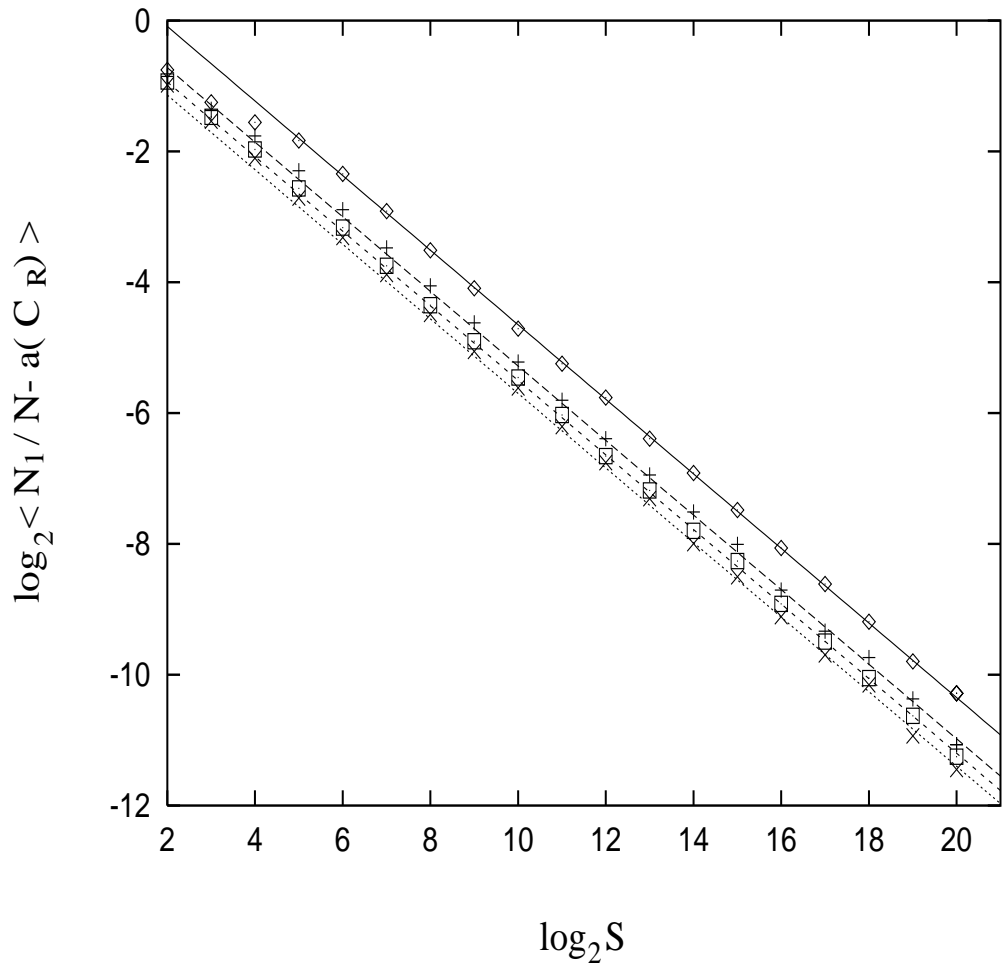


Fig. 15

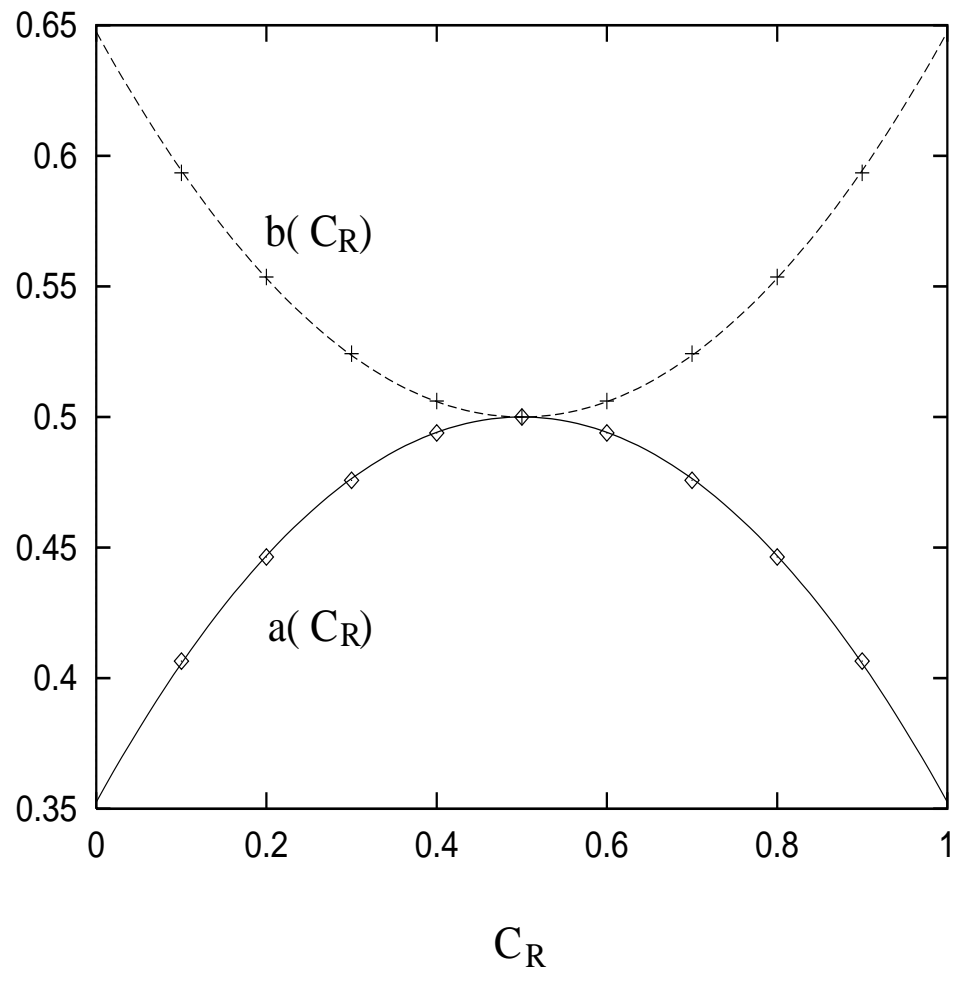


Fig. 16

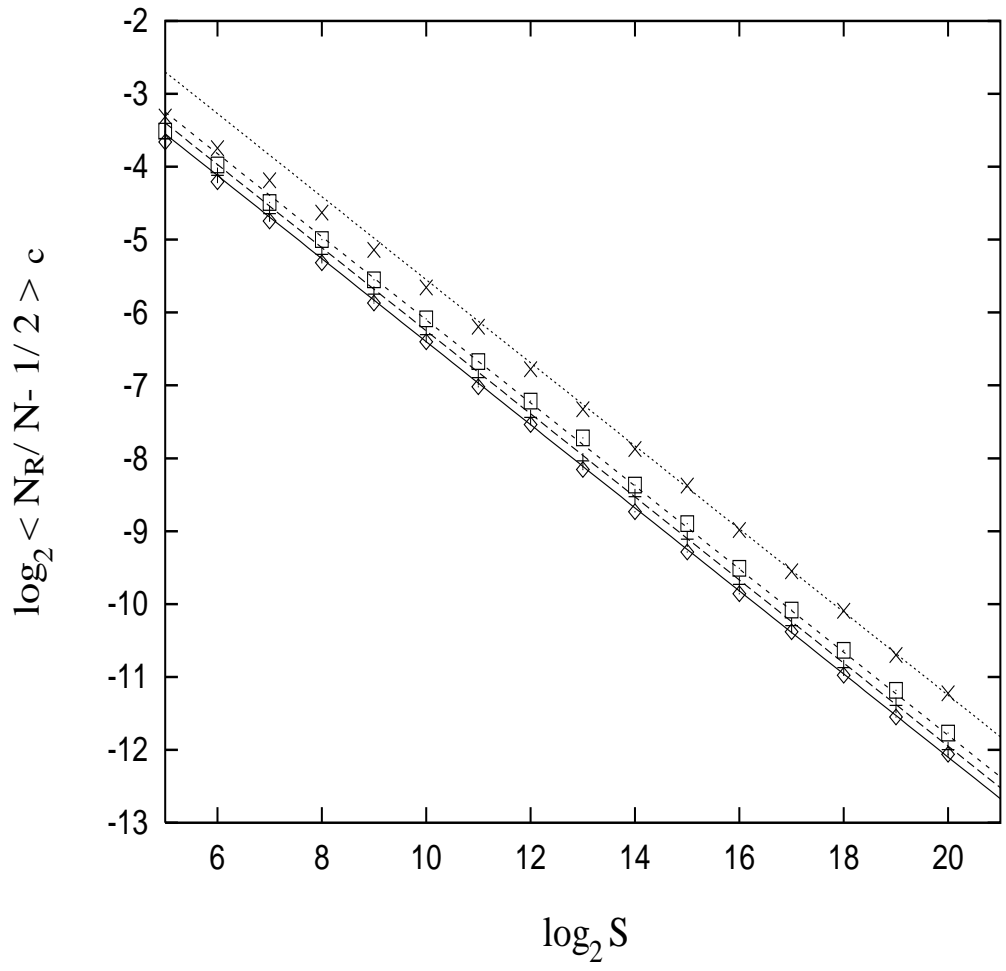


Fig. 17

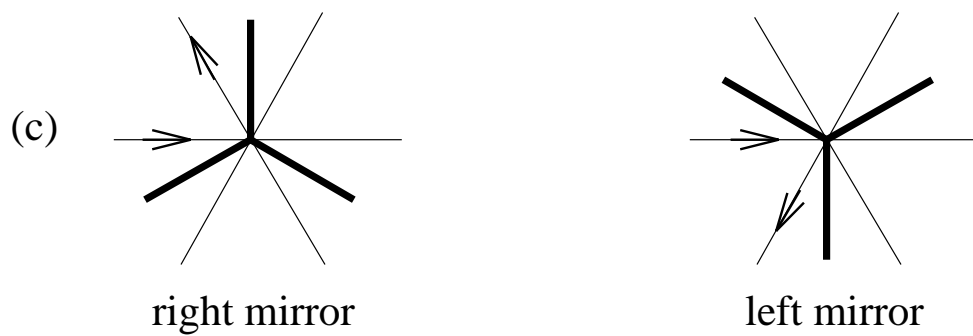
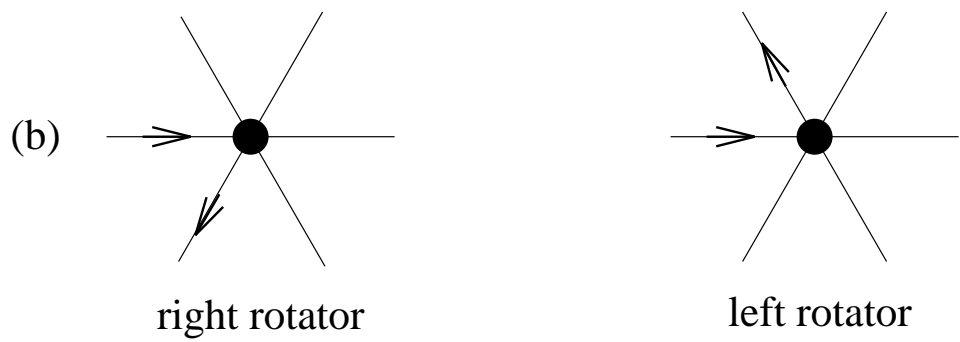
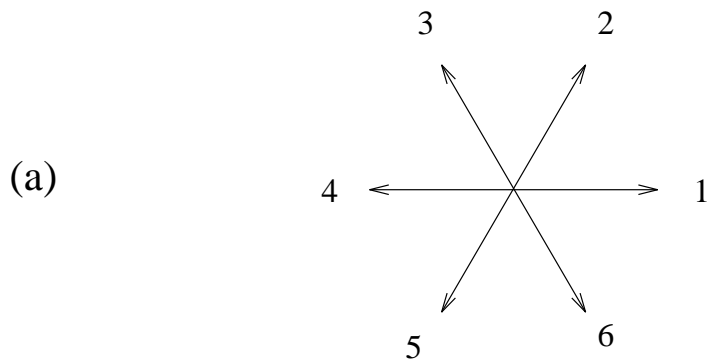


Fig. 18

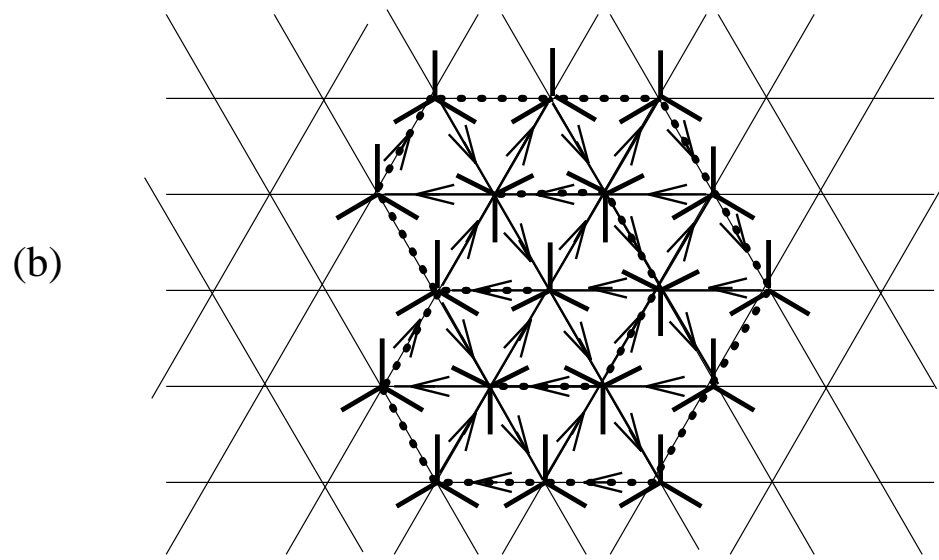
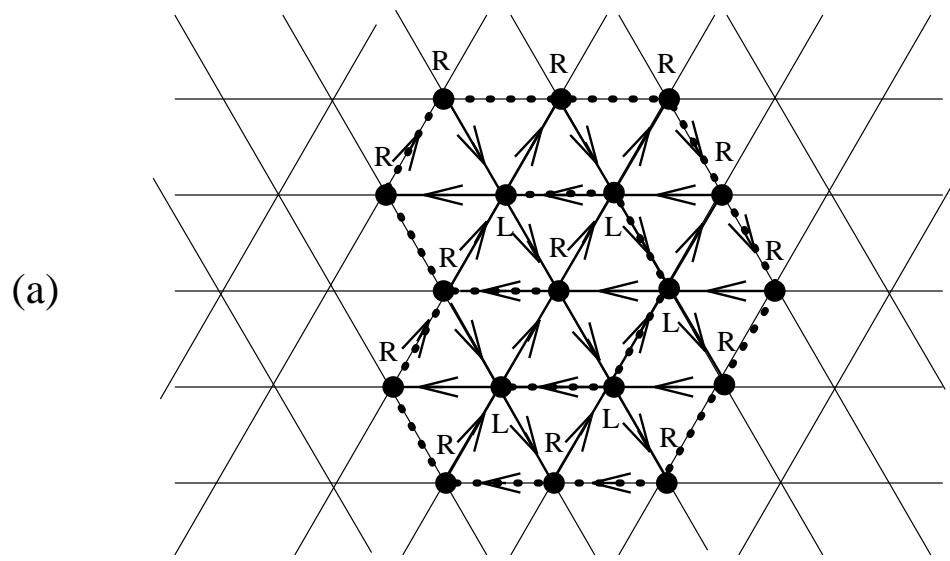


Fig. 19

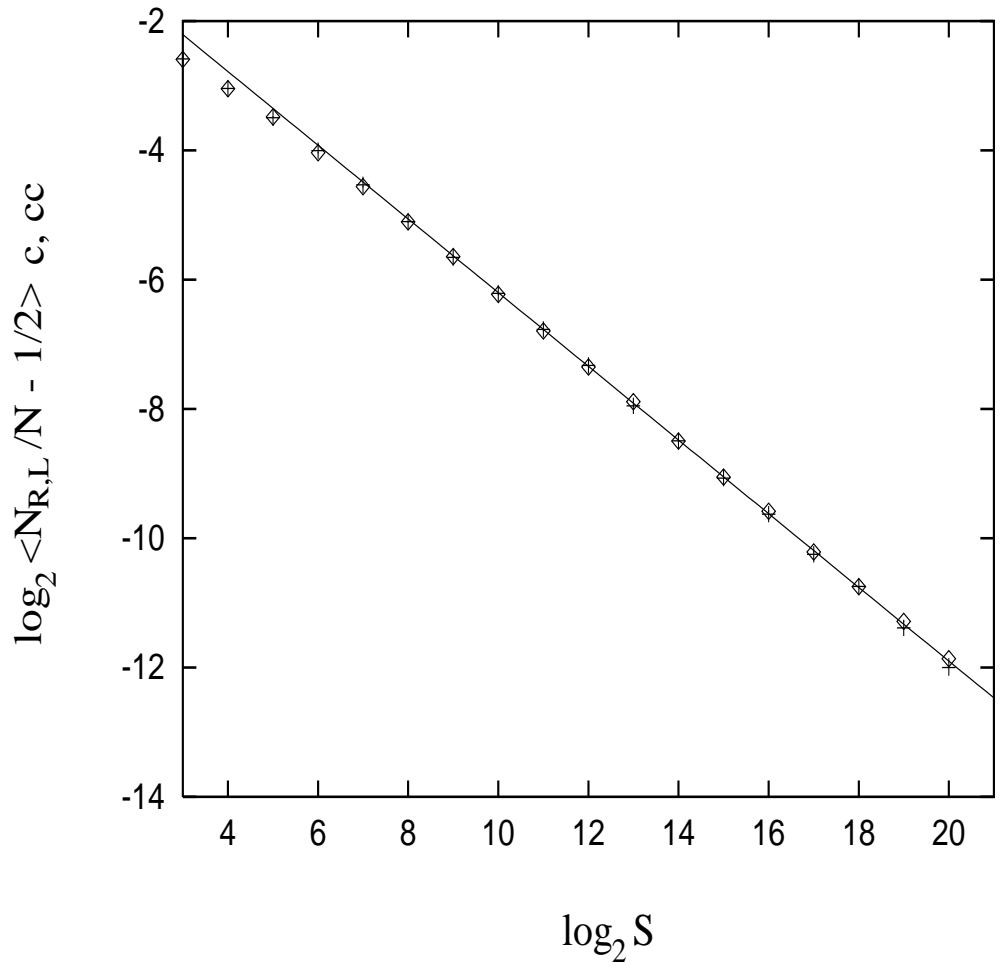


Fig. 20

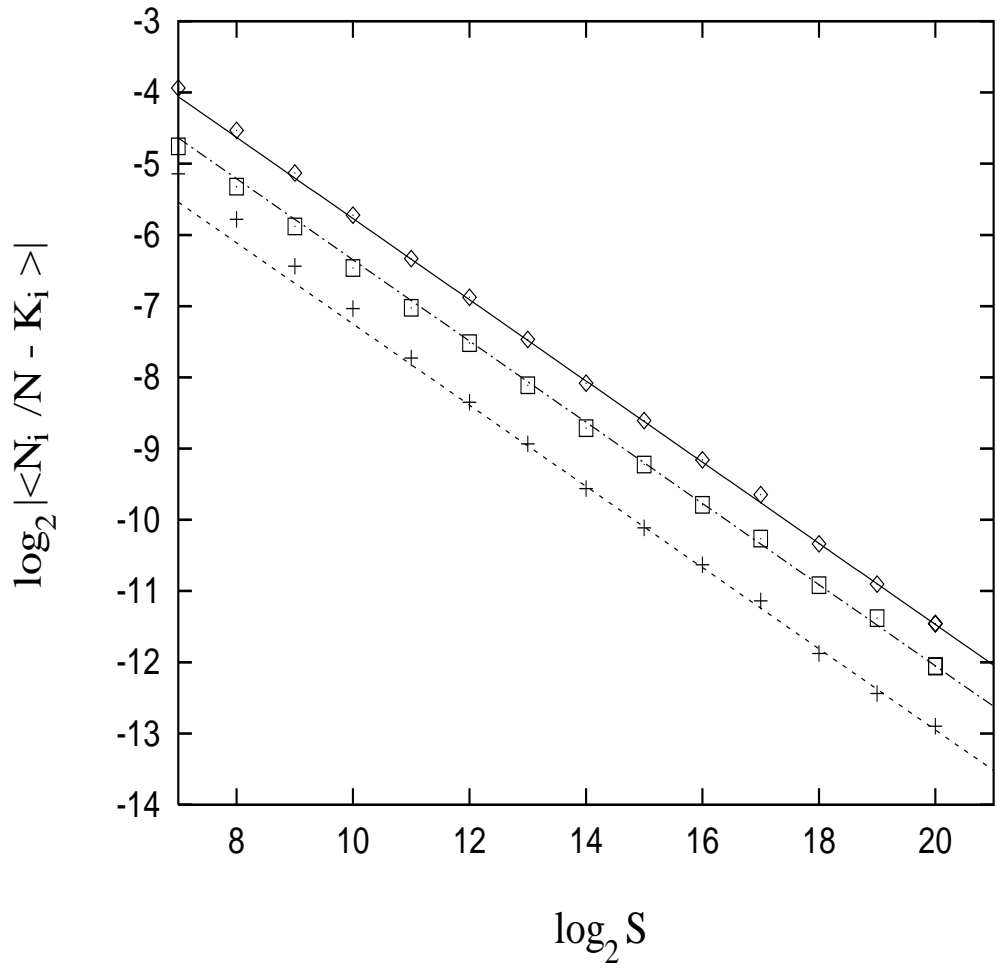


Fig. 21

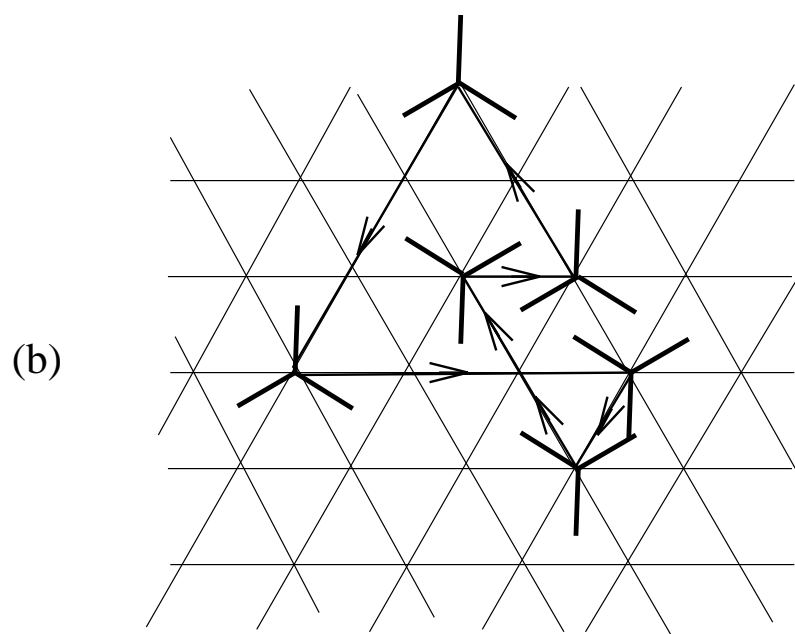
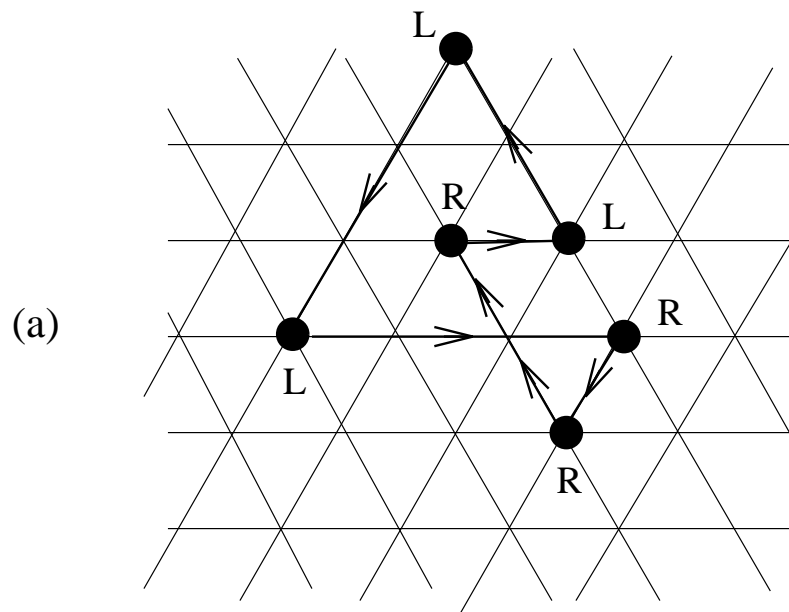


Fig. 22

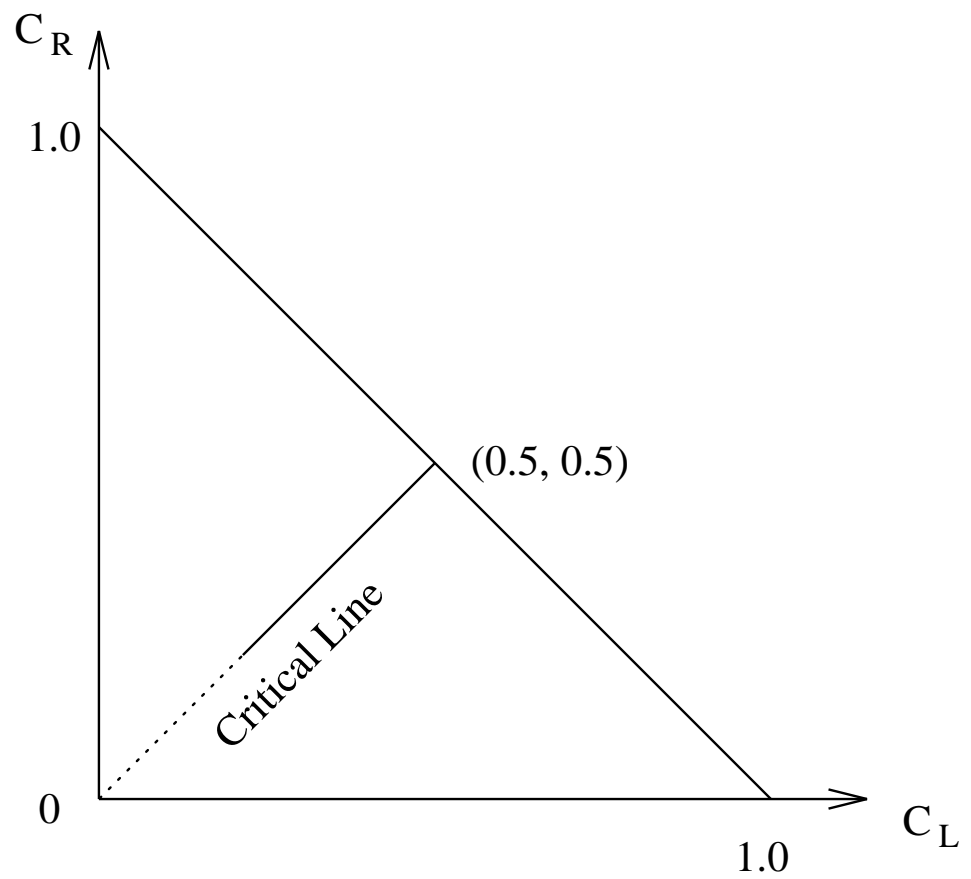


Fig. 23

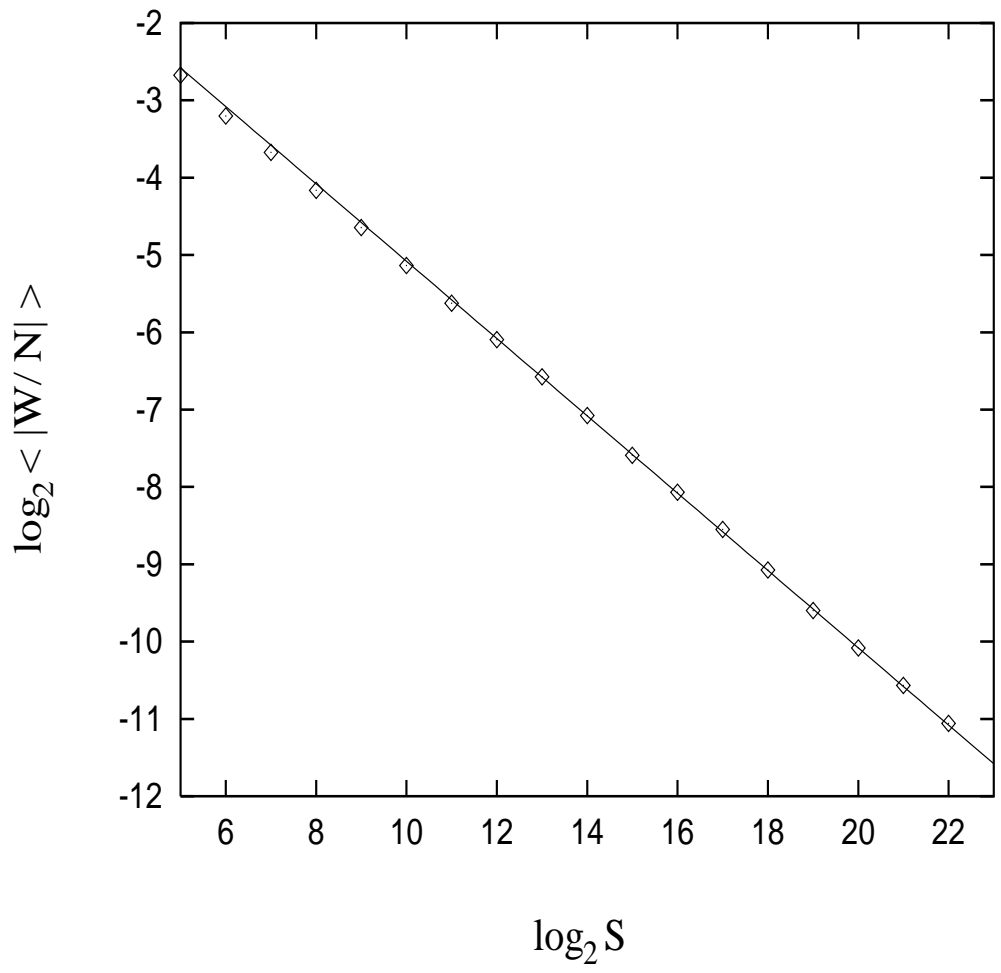


Fig. 24

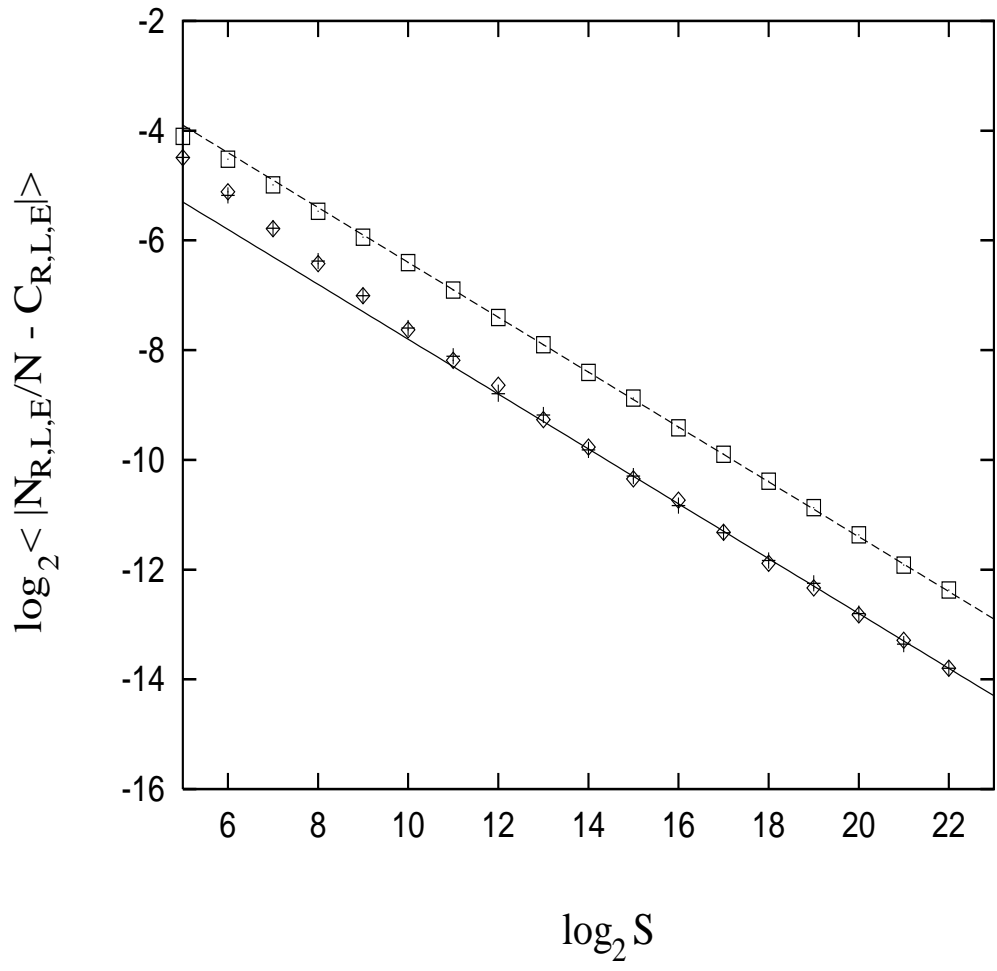


Fig. 25

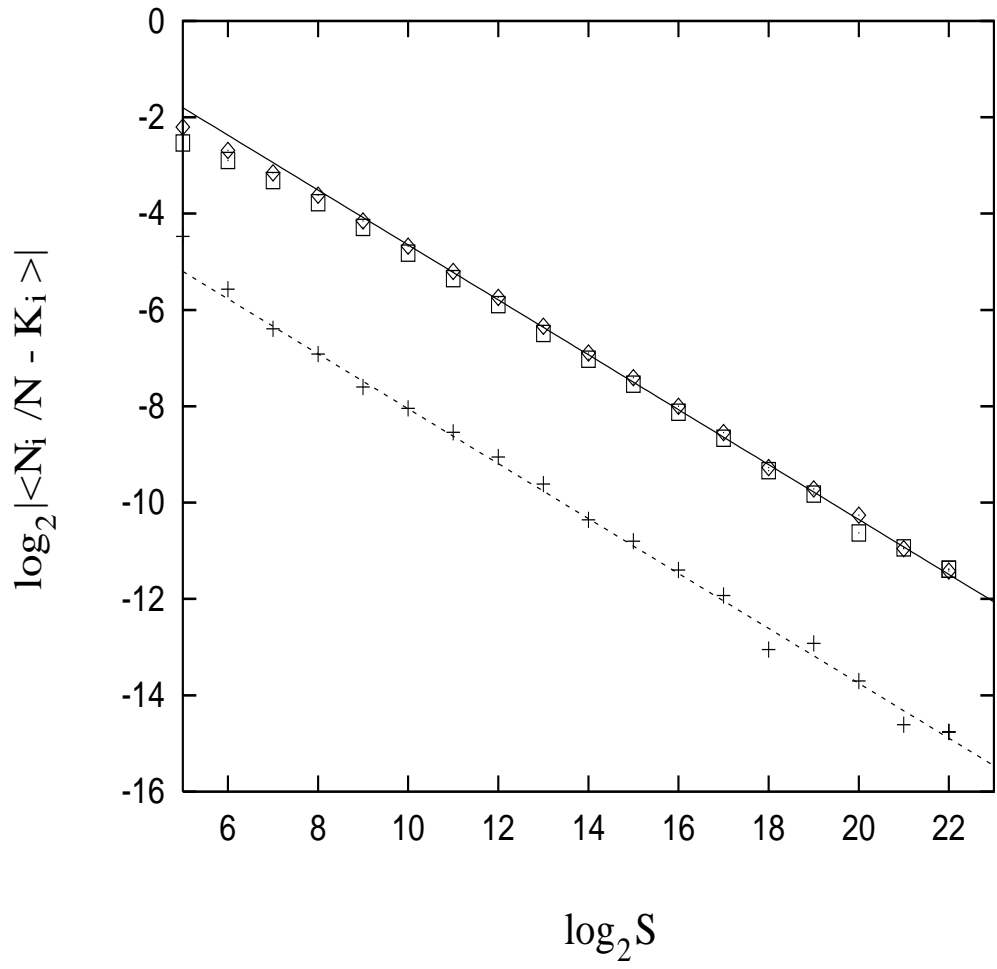


Fig. 26

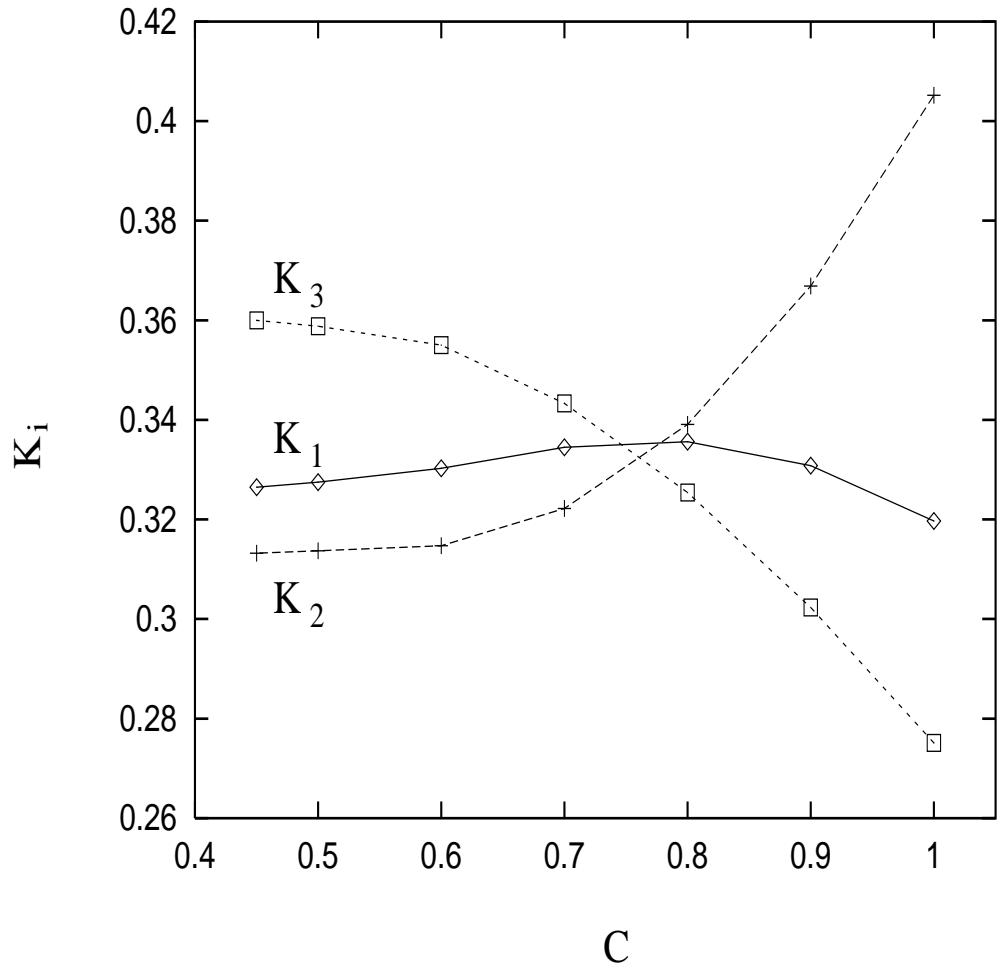


Fig. 27